frontiers in Materials

REVIEW
published: 17 July 2020
doi: 10.3389/fmats.2020.00213

Cerium and Its Oxidant-Based Nanomaterials for Antibacterial Applications: A State-of-the-Art Review

Manlin Qi[1†], Wen Li[1†], Xufeng Zheng[1], Xue Li[1,2], Yue Sun[1,2], Yu Wang[1], Chunyan Li[2,3] and Lin Wang[1,2]**

[1] Department of Oral Implantology, Hospital of Stomatology, Jilin University, Changchun, China, [2] Jilin Provincial Key Laboratory of Sciences and Technology for Stomatology Nanoengineering, Changchun, China, [3] Department of Prosthodontics, Hospital of Stomatology, Jilin University, Changchun, China

OPEN ACCESS

Edited by:
Denis Kuznetsov, National University of Science and Technology MISiS, Russia

Reviewed by:
Saeid Kargozar, Mashhad University of Medical Sciences, Iran
Geetha Manivasagam, VIT University, India

***Correspondence:**
Chunyan Li
cyli@jlu.edu.cn
Lin Wang
wanglin1982@jlu.edu.cn

† These authors have contributed equally to this work

Specialty section:
This article was submitted to Biomaterials, a section of the journal Frontiers in Materials

Received: *27 April 2020*
Accepted: *10 June 2020*
Published: *17 July 2020*

Citation:
Qi M, Li W, Zheng X, Li X, Sun Y, Wang Y, Li C and Wang L (2020) Cerium and Its Oxidant-Based Nanomaterials for Antibacterial Applications: A State-of-the-Art Review. Front. Mater. 7:213. doi: 10.3389/fmats.2020.00213

Infectious diseases caused by bacteria remain a serious and global problem in human health. Herein, the discovery and application of antibiotics, which has attracted much attention in the past years, has helped to cure numerous infectious diseases and made huge contributions in the biomedical field. However, the widespread use of the broad-spectrum antibiotics has led to serious drug resistance for many human bacterial pathogens. In particular, bacterial drug resistance decreases therapeutic effects and leads to high mortality. Inspiringly, the introduction of nanomaterials in the biomedical field makes it possible to overcome the difficulty in bacterial drug resistance attributed to their unique antibacterial mechanism. Recently, a variety of metal- and metal oxide-based nanomaterials have been fully integrated in antibacterial applications and achieved excellent performances. Among them, cerium- and cerium oxide-based nanomaterials have received much attention worldwide. Remarkably, cerium oxide nanoparticles with lower toxicity act as effective antibacterial agents owing to their unique functional mechanism against pathogens through the reversible conversion of oxidation state between Ce(III) and Ce(IV). This article provides an overview of the state-of-the-art design and antibacterial applications of cerium- and cerium oxide-based materials. The first part discusses the underlying antibacterial mechanisms for cerium- and cerium oxide-based materials currently applied in biomedicine. The second part focuses on various antibacterial-related materials and their applications. In addition, the existing problems and future perspectives of the cerium- and cerium oxide-based materials make up the third part of this review. This paper could provide the possible mechanisms for antibacterial activities, various designs of cerium- and cerium oxide-based materials, and related antibacterial properties.

Keywords: cerium, ceria, biomaterials, antibacterial, infectious disease

INTRODUCTION

During the past few hundred years, infectious diseases have been a persistent global and critical health problem, which has attracted considerable public attention worldwide as a human health threat (Jones et al., 2008; Fauci and Morens, 2012). Due to the high morbidity and mortality burden of infectious diseases, lots of investigations have focused on the aspects of understanding, controlling, treating, and preventing them for centuries (Casadevall et al., 2004; Matsuzaki et al., 2005; Fauci and Morens, 2012; Caliendo et al., 2013). Since the discovery of penicillin, which could be regarded as a significant contribution in the medical field (Gaynes, 2017), the therapeutic method of antibiotics has played an important role in addressing the issue of human infectious diseases (Nigam et al., 2014). However, the widespread use and abuse of antibiotics have caused the emergence of drug resistance, accompanied with limited treatment efficacy (D'Costa et al., 2011; Frieri et al., 2017). Therefore, it is urgent to develop novel antimicrobial agents to tackle the current challenges in treating infectious diseases, which can kill bacteria efficiently and with biosafety.

Recently, the development of nanomaterials and nanotechnology, which have already been used in a wide range of applications such as in agriculture (Khot et al., 2012), the environment (Das et al., 2015), analytical chemistry (Scida et al., 2011), and electronics and sensors (Chaudhary and Mehta, 2014), has attracted great interest. Owing to the specific structure and tailorable physicochemical properties of nanomaterials, they are regarded as promising materials utilized in the fields of biomedical research (Mitragotri et al., 2015). There are plenty of investigations on metal and metal oxide nanoparticles (NPs), such as silver (Franci et al., 2015), copper (Rodhe et al., 2015), copper oxide (CuO) (Ivask et al., 2014), titanium dioxide (TiO_2) (Jayaseelan et al., 2013), and zinc oxide (ZnO) (Sirelkhatim et al., 2015), which all showed outstanding antibacterial activities. The application of antibacterial agents against infectious diseases needs not only excellent bacterial killing efficacy but also lower or even no toxicity to the human normal cells. However, the biocompatibility of most nanomaterials is not ideal. For example, silver NPs with good antibacterial effect have been incorporated into some materials serving as an antibacterial component, but they have serious biosafety problems and easily causes cytotoxicity, which have limited their applications for human health care (Ávalos Fúnez et al., 2013).

Cerium dioxide (CeO_2), as a rare-earth material, has a variety of properties at the nanoscale and can be widely used as polishing agents (Chen et al., 2015), solid oxide fuel cells (Li et al., 2018; Sun et al., 2018), catalysts (Zhang et al., 2017), solar cells (Hu et al., 2018), and pharmacological agents (Charbgoo et al., 2017). Due to their lower toxicity to mammalian cells and unique antibacterial mechanism, CeO_2 NPs have also been widely applied in biomedical sciences such as in antitumor (Corsi et al., 2018), anti-inflammation (Huang F. et al., 2018; Huang X. et al., 2018), and antibacterial activities (Arumugam et al., 2015), in combating neurodegenerative diseases (Naz et al., 2017), and as immunosensors (Naz et al., 2017). Remarkably, CeO_2 have shown promising approaches to circumvent the existing problems of drug-resistant bacteria and served as excellent antibacterial agents in biology and medical sciences in comparison with other metal oxides (Zhang et al., 2019). However, it was found that CeO_2 NPs at low concentrations (1 mg/L) could not destroy the bacterial biofilms (Hou et al., 2015). Therefore, various cerium- and cerium oxide-based nanomaterials including doping metal ions (Atif et al., 2019), antibacterial element Au/Ag decorations (Babu et al., 2014; Wang et al., 2014), nanocontainers (Gagnon et al., 2015), dopants (Bomila et al., 2018), and a component of blend (Pandey et al., 2018a) were developed to optimize antimicrobial performance as well as physical and biological properties (Anastasiou et al., 2019; Bharathi and Stalin, 2019; Liu et al., 2019).

In recent years, numerous valuable reviews on cerium and its oxides have been published, focusing on the synthesis (Nyoka et al., 2020), catalysis (Walkey et al., 2015), defect engineering (Seal et al., 2020), pharmaceutical properties (Xu and Qu, 2014), and biological and biomedical effects (Dhall and Self, 2018; Kargozar et al., 2018; Zhang et al., 2019; Casals et al., 2020). Nevertheless, the antibacterial effects of cerium and its oxides with different material designs, particularly on infectious diseases, were rarely reviewed. Therefore, this review began with a brief introduction of the antibacterial mechanism of CeO_2 NPs, followed by summarizing the various designs of cerium- and cerium oxide-based nanomaterials. In addition, this article presented a comprehensive overview of new developments in the antibacterial applications of cerium- and cerium oxide-based nanomaterials against infectious diseases and would provide guidance to develop new cerium-related antibiotics in the future.

ANTIBACTERIAL MECHANISM OF CERIUM-BASED MATERIALS

Nowadays, cerium has been verified to possess the potential to serve as an effective and long-lasting biocide for preventing bacterial infections, due to its higher safety to human cells and unique antibacterial mechanism compared with other metal ions. Cerium- and cerium oxide-based antimicrobials have attracted tremendous attention, and many studies have reported various kinds of designs about the cerium-related nanomaterials against microorganisms, which will be detailed in the latter part. The main antibacterial mechanism for CeO_2 can be attributed to the direct contact between CeO_2 and bacterial membranes. The schematic representation of antibacterial mechanism of cerium-based materials is shown in **Figure 1**.

First, the positively charged NPs were adsorbed onto the membranes of negatively charged Gram-positive and Gram-negative bacteria through electrostatic interaction. Due to the electrostatic interaction and bacterial membrane blocking, the NPs persisted on the surface of bacteria for a long time rather than penetrating the membrane. Afterward, NPs may change the viscosity of the membrane, impair the specific ionic pumps, and eventually strongly change the transport exchanges between the bacterial cell and the solution to disturb bacterial growth (Thill et al., 2006).

Second, CeO_2 could attack proteins after adsorbing on the outer membrane of the bacterial cell. The released cerium ions could alter electron flow and respiration of bacteria (Pelletier et al., 2010) and react with the thiol groups (–SH) or be absorbed onto transporters and/or porins to hamper nutrient transportation (Zeyons et al., 2009; Li et al., 2019b). In addition, the irregular shapes and rough edges of CeO_2 *per se* contribute to

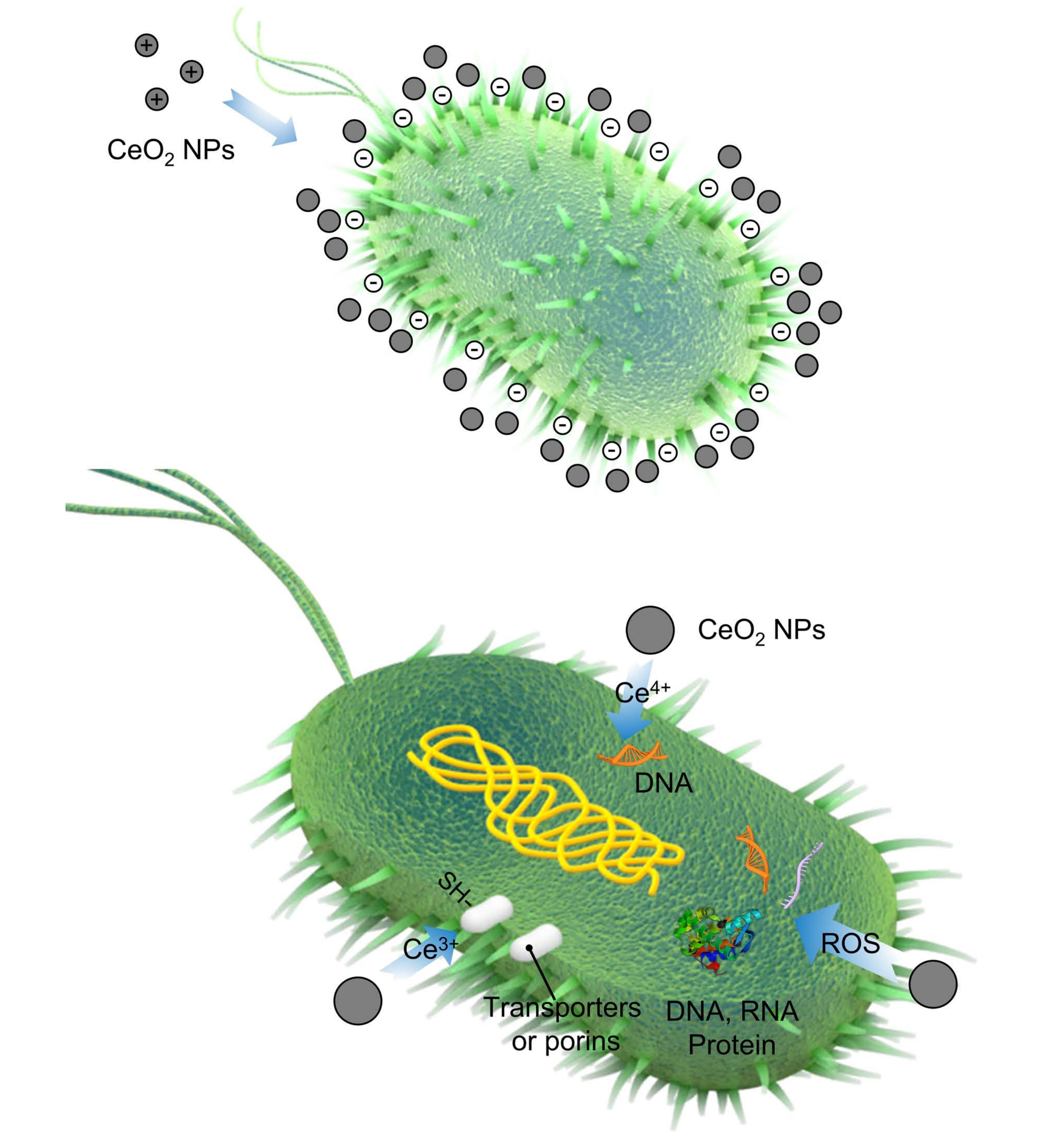

FIGURE 1 | The schematic representation of the antibacterial mechanism of cerium-based materials.

the physical damage of bacterial membranes, especially for Gram-positive bacteria (Arumugam et al., 2015; Zhang et al., 2019).

Third, oxidative stress is also an important factor for CeO_2 during the antibacterial process. Generally, oxidative stress was induced by the generation of reactive oxygen species (ROS) *in vivo*, whereas the ROS generated was induced by the reversible conversion between Ce(III) and Ce(IV) on the surface of bacterial membranes (Zhang et al., 2019). The ROS can attack the nucleic acids, proteins, polysaccharides, lipids, and other biological molecules to cause the loss of their function, eventually killing and decomposing bacteria (Li et al., 2012). Although CeO_2 can be excited to produce ROS by ultraviolet (UV) irradiation, there were very few researches on bacterial activity by using CeO_2 alone. Usually, CeO_2 combined with other photocatalysts like TiO_2. In the presence of CeO_2, the band gap can be changed in the host lattices of photocatalysts, which improves the photocatalytic activity of TiO_2 (Kasinathan et al., 2016).

Finally, Ce(IV) ion could induce hydrolysis of a DNA oligomer into the fragments, which then could be successfully manipulated by natural enzymes (Sumaoka et al., 1998). Extracellular DNA (eDNA) is one of the important components in the process of biofilm formation, making the biofilm hard to eliminate. Therefore, taking advantage of Ce-based nanozymes with deoxyribonuclease (DNase) mimetic activity could lead to high cleavage ability toward eDNA and disrupt established biofilms (Chen et al., 2016; Liu et al., 2019).

CERIUM OXIDE AND COMPOUNDS CONTAINING CERIUM

Cerium Oxide for Antibacterial Application

This part mainly reviewed the antibacterial effect of pure CeO_2 with different morphologies in recent years. The details are summarized in **Table 1**, and parts of TEM or SEM images of CeO_2 with different morphologies are shown in **Figure 2**. Spherical-shaped CeO_2 NPs showed antibacterial activity against Gram-negative bacteria *Escherichia coli* (*E. coli*) and *Pseudomonas aeruginosa* (*P. aeruginosa*) and less or no antibacterial activity against Gram-positive bacteria *Staphylococcus aureus* (*S. aureus*) (Ravishankar et al., 2015; Selvaraj et al., 2015; Surendra and Roopan, 2016; Senthilkumar et al., 2019), because of the direct contact onto the membrane surface of *E. coli* that blocks the synthesis of the cell wall and membrane and disturbs other cellular processes (Senthilkumar et al., 2019). Similarly, it was found that the CeO_2 NPs showed superior activity against Gram-negative *E. coli* than Gram-positive *Bacillus subtilis* (*B. subtilis*), which has a slight reduction in survival (Patil et al., 2016). However, in other studies, the spherical-shaped CeO_2 NPs with a smaller size showed contradictory antibacterial effects (Arumugam et al., 2015; Arunachalam et al., 2018). The CeO_2 NPs showed mild and moderate antibacterial behavior against Gram-negative *P. aeruginosa* and *Proteus vulgaris* (*P. vulgaris*) with a zone of inhibition (ZOI) of 4.09 ± 0.22 and 4.38 ± 0.44 mm, respectively, whereas they had highly potent antibacterial behavior against Gram-positive *S. aureus* and *Streptococcus pneumoniae* (*S. pneumoniae*) with a ZOI of 12.43 ± 0.36 and 14.56 ± 0.23 mm, respectively. The authors thought various factors such as smaller-sized particles, rigid morphology, surface interaction, and variation in the band gap energy of CeO_2 NPs contributed to the antimicrobial activity (Arunachalam et al., 2018). Arumugam et al. (2015) thought that the uneven ridges and oxygen defects of CeO_2 NPs led to these inconsistent results. A similar antibacterial activity was found in CeO_2 NPs with irregular morphologies and poor dispersity (Yadav et al., 2016).

CeO_2 microspheres by green synthesis showed significant antibacterial activity against *E. coli* and *S. aureus* with ZOI values of 4.67 and 3.33 mm, respectively. The ZOI depends on the type of bacteria, the concentration, surface area, shape, and size of NPs. Besides, the structural and configurational differences of the cell membrane lead to the difference of antibacterial effect against different types of bacteria (Malleshappa et al., 2015). The inhibition effect of CeO_2 nanocube is *B. subtilis* > *Enterococcus faecalis* (*E. faecalis*) = *Salmonella typhimurium* > *E. coli*. Moreover, they found that interaction between CeO_2 nanocubes and *E. coli* led to bacterial cell wall damage or disruption by detected β-D-galactosidase which is present in *E. coli* (Krishnamoorthy et al., 2014). Interestingly, it was reported that CeO_2 nanosheets exhibited stronger antibacterial activity compared with the CeO_2 NPs. In the synthesis process, the former route is the same, and the CeO_2 nanosheets were formed by hydrothermal treatment, while the CeO_2 NPs were synthesized by washing and annealing. The CeO_2 nanosheets showed a higher surface area, leading to a higher concentration of oxygen vacancies on the surface, which caused enhanced ROS generation. Therefore, CeO_2 nanosheets exhibited stronger antibacterial activity (Abbas et al., 2016).

Living conditions such as solution pH and phosphate solution could also affect the bacteriostatic effect. Dextran-coated CeO_2 NPs were much more effective against *P. aeruginosa* and *Staphylococcus epidermidis* (*S. epidermidis*) at basic pH values (pH = 9) compared with acidic pH values (pH = 6). The size of CeO_2 NPs is smaller and have a positive charge at pH = 9, whereas CeO_2 NPs show a negative charge at pH = 6. These properties at an alkaline pH make CeO_2 NPs easier to absorb on the bacteria and achieve a favorable antibacterial effect (Alpaslan et al., 2017). It was believed that CeO_2 NPs with a lower Ce^{3+}/Ce^{4+} ratio show antibacterial activity (Gupta et al., 2016), but in a phosphate solution, it showed that CeO_2 NPs in the (III) oxidation state had a significant antibacterial activity other than those in the (IV) oxidation state. Exposure of *E. coli* to the equimolar mixture of CeO_2 NPs in the (III) oxidation state and phosphate for 3 h resulted in ∼90% reduction. However, the equimolar mixture of CeO_2 NPs in the (IV) oxidation state and phosphate for a long time did not show significant bacterial reduction (Sargia et al., 2017).

Apart from pure CeO_2, cerium oxide containing some elements also showed antibiotic activity. $CeVO_4$ NPs showed excellent antibacterial activity against *Streptococcus mutans* and *Streptococcus pyogenes* with minimum inhibitory concentration (MIC) values at 200 μg/ml and against *Vibrio cholera*, *Salmonella typhi*, and *Shigella flexneri* with MIC values at 350 μg/ml (Mishra et al., 2020).

Metal Element Doping Into Cerium Oxide NPs for Antibacterial Enhancement

Most transition metals have unfilled d-orbitals and thus are redox active. Their ability to easily cycle between oxidation states contributes to both their catalytic properties and their toxicity

TABLE 1 | Recent studies on cerium dioxide against various pathogens.

Design	Morphology	Dose and Conditions	Pathogens	Antimicrobial/Inhibition Activity		References
				Parameters	Antimicrobial Efficiency	
CeO_2	spherical	25 µl	*E. coil*	ZOI	7 mm	Surendra and Roopan, 2016
			S. aureus		5 mm	
	spherical	1, 10, 50, 100 mg/L	*E. coil*	ZOI	+	Selvaraj et al., 2015
			S. aureus		–	
	spherical	500 µg/50 µl	*P. aeruginosa*	ZOI	3.33 ± 0.33 mm	Ravishankar et al., 2015
		1,000 µg/50 µl			4.50 ± 0.29 mm	
		500 µg/50 µl	*S. aureus*		Not seen	
		1,000 µg/50 µl				
	spherical	20–60 µl	*E. coil*	ZOI	7–12 mm	Senthilkumar et al., 2019
	spherical	1–2 mM	*B. subtilis*	CFU reduction	60–85%	Patil et al., 2016
		1–2 mM	*E. coil*		70–95%	
	spherical	100 mg	*E. coli*	ZOI	4.00 mm	Arumugam et al., 2015
			S. dysenteriae		4.33 mm	
			P. aeruginosa		4.67 mm	
			P. vulgaris		4.67 mm	
			K. pneumoniae		4.67 mm	
			S. pneumoniae		4.67 mm	
			S. aureus		5.33 mm	
	spherical	100 mg/ml	*P. aeruginosa*	ZOI	4.09 ± 0.22 mm	Arunachalam et al., 2018
			P. vulgaris		4.38 ± 0.44 mm	
			S. aureus		12.43 ± 0.36 mm	
			S. pneumoniae		14.56 ± 0.23 mm	
	spherical	pH = 9	*P. aeruginosa*	LIVE/DEAD staining and TEM imaging	Reduction in cell number	Alpaslan et al., 2017
			S. epidermidis		Drastic morphological changes	
	cubic and spherical	5–10 mg/ml	*E. coli*	ZOI	3.33 ± 0.33 to 6.33 ± 0.33 mm	Gopinath et al., 2015
			S. pneumoniae		3.33 ± 0.33 to 10.67 ± 0.33 mm	
			P. vulgaris		3.67 ± 0.33 to 8.33 ± 0.33 mm	
			B. subtilis		4.67 ± 0.33 to 10.33 ± 0.33 mm	
	microspheres	500 µg/50 µl to 1,000 µg/100 µl	*P. desmolyticum*	ZOI	1.00 ± 0.00 to 1.67 ± 0.33 mm	Malleshappa et al., 2015
			K. aerogenes		1.00 ± 0.00 to 2.33 ± 0.33 mm	
			S. aureus		1.67 ± 0.33 to 3.33 ± 0.67 mm	
			E. coli		2.67 ± 0.33 to 4.67 ± 0.33 mm	
CeO_2	nanocubes	N/A	*B. subtilis*	MIC	4 µg/ml	Krishnamoorthy et al., 2014
			E. faecalis		8 µg/ml	
			S. typhimurium		8 µg/ml	
			E. coli		16 µg/ml	
	nanosheets	N/A	*E. coil*	ZOI	++	Abbas et al., 2016
			S. aureus		+	
	irregular	500 µg/50 µl	*K. aerogenes*	ZOI	Inactive	Yadav et al., 2016
		1,000 µg/100 µl			1.00 ± 0.00 mm	
		500 µg/50 µl	*S. aureus*		0.53 ± 0.12 mm	
		1,000 µg/100 µl			1.47 ± 0.03 mm	
	nanoparticles	100–200 µg/ml	*P. aeruginosa*	ZOI	15 ± 1.0 to 25 ± 0.5 mm	Roudbaneh et al., 2019
			K. pneumoniae		28 ± 1.0 to 35 ± 0.5 mm	
			E. coli		31 ± 1.0 to 37 ± 0.5 mm	
			S. aureus		31 ± 0.5 to 37 ± 0.5 mm	
	nanoparticles	100 mg/ml	*E. coli*	ZOI	1.7 cm	Kumar et al., 2018
			B. subtilis		1.8 cm	

(Continued)

TABLE 1 | Continued

Design	Morphology	Dose and Conditions	Pathogens	Antimicrobial/Inhibition Activity		References
				Parameters	Antimicrobial Efficiency	
	nanoparticles	sonication time 0–120 (min)	*E. coli*	MIC	1,000–3,000 μg/ml	Sanhueza et al., 2019
			S. aureus		3,000 μg/ml	
$CeVO_4$	nanoparticles	N/A	*S. mutans*	MIC	200 μg/ml	Mishra et al., 2020
			S. pyogenes		200 μg/ml	
			V. cholera		350 μg/ml	
			S. typhi		350 μg/ml	
			S. flexneri		350 μg/ml	

B. cereus, Bacillus cereus; B. subtilis, Bacillus subtilis; E. coli, Escherichia coli; E. faecalis, Enterococcus faecalis; K. aerogenes, Klebsiella aerogenes; K. pneumoniae, Klebsiella pneumoniae; MIC, minimum inhibitory concentration; P. aeruginosa, Pseudomonas aeruginosa; P. desmolyticum, Pseudomonas desmolyticum; P. vulgaris, Proteus vulgaris; S. aureus, Staphylococcus aureus; S. dysenteriae, Shigella dysenteriae; S. epidermidis, Staphylococcus epidermidis; S. flexneri, Shigella flexneri; S. mutans, Streptococcus mutans; S. pneumoniae, Streptococcus pneumoniae; S. pyogenes, Streptococcus pyogenes; S. typhi, Salmonella typhi; S. typhimurium, Salmonella typhimurium; V. cholera, Vibrio cholera; ZOI, zone of inhibition.

(Palmer and Skaar, 2016). In a recent study, different transition metal ions (Fe^{2+}, Mn^{2+}, and Co^{2+}) doped with nanosized hydroxyapatite (HA) were prepared for the increase of load-bearing capacity and strength; meanwhile, higher antibacterial activities were achieved against most tested bacteria compared with erythromycin (Panneerselvam et al., 2020). These transition metal elements (Fe, Mn, and Co) were also separately doped into CeO_2 NPs and proven to have enhanced antimicrobial activities (Khadar et al., 2019; Atif et al., 2019; Rahdar et al., 2019). The metal ions were placed into the atomic site of the Ce ions and substituted in the matrix of the host CeO_2. The bonding of metal ions with CeO_2 NPs was formed (Khadar et al., 2019; Atif et al., 2019; Rahdar et al., 2019). The antibacterial activity of various transition metal-doped metal oxide nanostructures comes from an electrostatic induction nature between NPs and the bacterial cell membrane (Khadar et al., 2019). The synergetic effects of transition metal doped into CeO_2 NPs increase the antibacterial activity caused by ROS. Doping a certain amount of trivalent rare-earth metals could decrease the lattice parameter to enhance the antibacterial efficiency of CeO_2 NPs. Among the lanthanide series, samarium ion (Sm^{3+}) could increase active oxygen vacancies in the CeO_2 NPs and had properties of high-intensity optical, electrical, and antimicrobial activities (Artini et al., 2015). The antibacterial activities were found increased as the amount of metal dopants increased (Artini et al., 2015; Atif et al., 2019; Khadar et al., 2019). However, all of these experiments had a common problem: they did not evaluate or only evaluated the toxicity of cancer cells instead of normal cells.

Antibacterial Element Incorporation/Modification for Antibacterial Amplification

Recently, silver NPs and silver compounds have attracted more and more researchers' attention because of their efficient antimicrobial activities toward both Gram-positive (Li et al., 2020) and Gram-negative (Ramalingam et al., 2016) bacteria as well as fungi (Ballottin et al., 2017). The multifaceted mode of action of Ag^+ against bacteria makes it impossible to cause a high-level, single-step, target-based mutation to silver resistance (Chopra, 2007). Instead, this property makes sliver-based drugs a potential alternative to antibiotics.

CeO_2 nanorods, nanocubes, and NPs were synthesized, and different proportions of Ag^+ were incorporated in CeO_2, forming Ag/CeO_2 (Wang et al., 2014). CeO_2 nanocubes and nanorods achieved much higher bactericidal activities due to exposed crystal planes and oxidation ability. After loading with a small amount of Ag, the bactericidal activities were largely increased by both extracellular and intracellular ROS. *E. coli* treated with Ag/CeO_2 nanorods showed the highest relative ROS level, while those treated with Ag/CeO_2 NPs exhibited the lowest relative ROS level. The redox cycle of Ag^+/Ag^0 and Ce^{3+}/Ce^{4+} co-maintained the catalytic process of extracellular ROS formation, and Ag^+ also promoted the generation of intracellular ROS through respiratory enzymes (Wang et al., 2014). Negi et al. (2019) synthesized Ag/CeO_2 nanostructured materials for inhibiting the growth of *S. aureus* and *P. aeruginosa*. The MIC values of Ag/CeO_2 against the aforementioned bacteria were 3.125 and 6.25 μg/ml, respectively. The observation results showed the significantly improved catalytic and antibacterial properties compared with pure CeO_2, probably since Ag weakened the Ce–O bond situated nearby and accelerated ROS generation to enhance the catalytic reactions (Negi et al., 2019).

Various semiconductors like TiO_2 and CeO_2 could be coupled with compounds derived from silver to enhance charge separation and induce photocatalytic activity under visible light. Eswar et al. (2015) synthesized CeO_2 by two different methods. The low-band-gap CeO_2 synthesized using the polyethylene glycol (PEG)-assisted sonochemical method was named P-CeO_2. The results of the photocatalytic degradation of *E. coli* using CeO_2, $CeO_2/AgBr$, CeO_2/Ag_3PO_4, $CeO_2/AgBr/Ag_3PO_4$, and P-$CeO_2/AgBr/Ag_3PO_4$ composites showed differently in the dark and under visible light (**Figure 3**). All the composites had at least 1 log colony-forming unit (CFU) reduction in the dark, and after eliminating the photolysis factor, all the composites had at least 3 log CFU extra reduction under visible light. Among them, the $CeO_2/AgBr/Ag_3PO_4$ composite showed a superior bactericidal efficiency compared to other composites

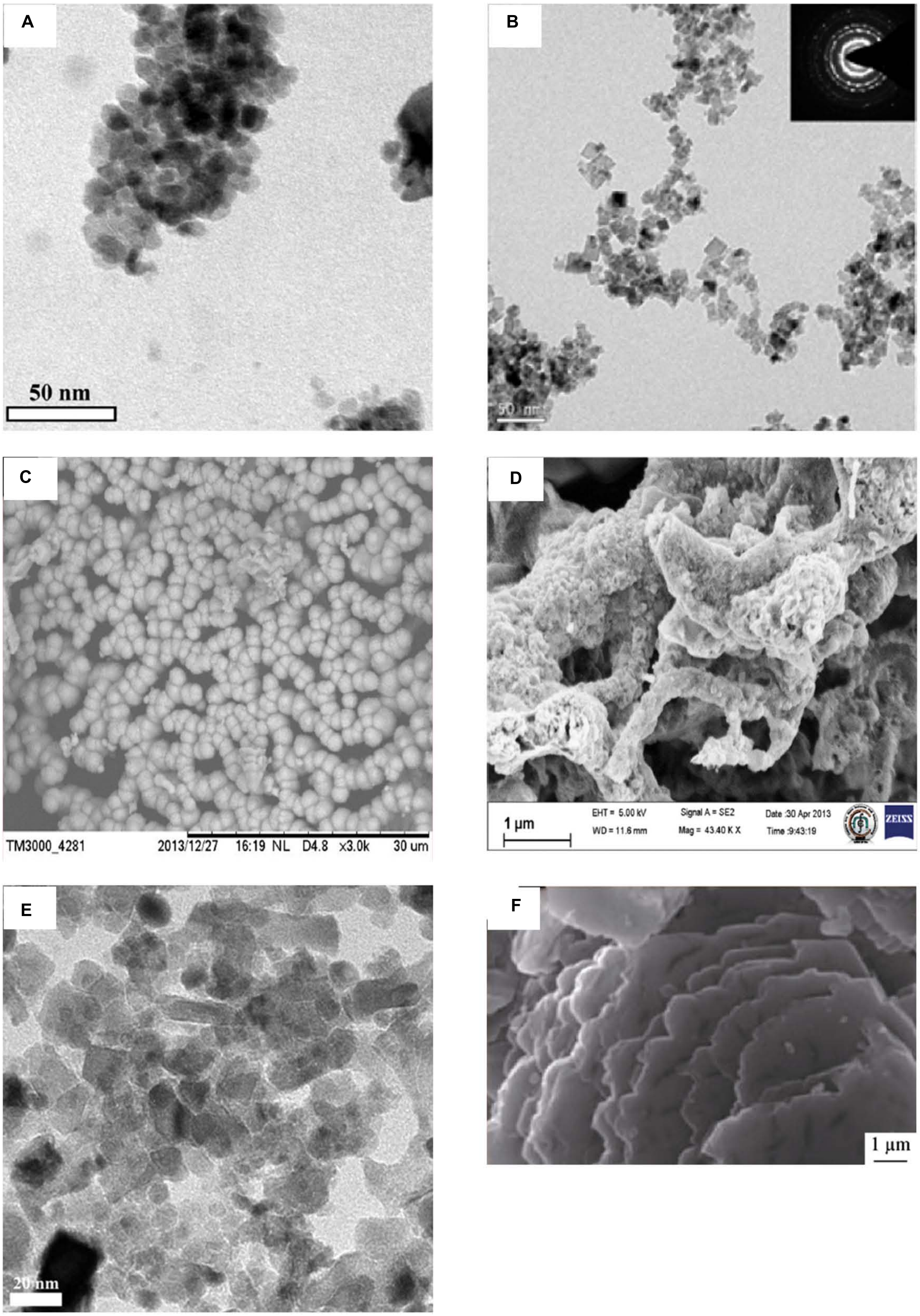

FIGURE 2 | Images of CeO_2 with various morphologies. **(A)** TEM images of spherical CeO_2 NPs. **(B)** The high-resolution transmission electron micrograph of CeO_2 nanocubes. The inset in **(B)** shows the corresponding SAED pattern. **(C)** SEM micrographs of microsphere CeO_2 NPs. **(D)** SEM images of irregular CeO_2 NPs. **(E)** TEM images of cubic and spherical mycosynthesized CeO_2 NPs calcinated at 400°C. **(F)** SEM images of prepared CeO_2 nanosheets. Reprinted with permission from Arumugam et al. (2015), copyright 2015 Elsevier, for panel **A**; Krishnamoorthy et al. (2014), copyright 2014 Elsevier, for panel **B**; Malleshappa et al. (2015), copyright 2015 Elsevier, for panel **C**; Yadav et al. (2016), copyright 2016 Springer, for panel **D**; Gopinath et al. (2015), copyright 2015 Springer, for panel **E**; and Abbas et al. (2016), Copyright 2016 Springer, for panel **F**.

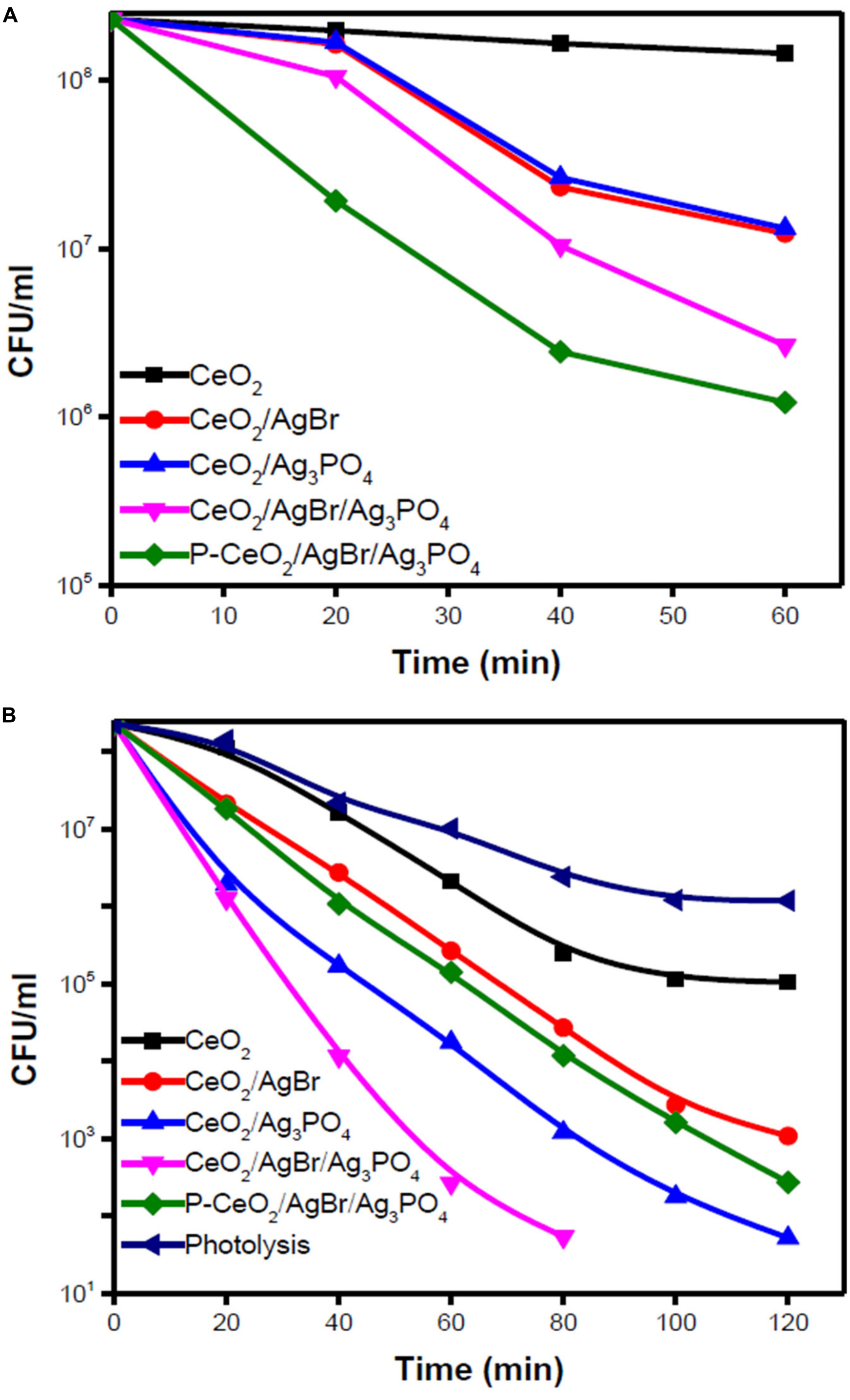

FIGURE 3 | Photocatalytic degradation of *Escherichia coli* using ceria/Ag_3PO_4, ceria/AgBr, and ceria/Ag_3PO_4/AgBr composites against **(A)** dark and **(B)** visible light. Reprinted with permission from Eswar et al. (2015), copyright 2015 American Chemistry Society.

under visible light due to ROS and elution of Ag^+ into the reaction system (Eswar et al., 2015).

However, most silver-based drugs have the disadvantages of a short-term antimicrobial activity and fast Ag^+ release and may increase the risk of impairing the surrounding tissues (Gagnon et al., 2016). Gagnon et al. designed CeO_2 nanocontainers that were used to encapsulate silver nitrate and silver NPs ($AgNO_3/CeO_2$ and $AgNP/CeO_2$ nanocontainers). $AgNO_3/CeO_2$ nanocontainers had a lower minimum bactericidal concentration (MBC) than $AgNP/CeO_2$ nanocontainers against

E. coli, indicating a higher antibacterial activity. Based on this, another nanocontainer, AgNP/CeO_2/TiO_2, was designed to control the Ag^+ release. After further encapsulation of TiO_2, only about 7% of total Ag load was released in 3 months, and the remaining Ag release was triggered by the oxidation of silver using nitric acid. Decrease of the pH caused by the bacterial metabolism in the environment could promote the oxidation of Ag and increase the Ag^+ release. This design could function as antimicrobial coatings to prevent implant infection. However, compared to AgNP/CeO_2 nanocontainers, AgNP/CeO_2/TiO_2 nanocontainers gained increased cytotoxicity toward a model epithelial barrier cell type (A549 cells) (Gagnon et al., 2016).

Au NPs were regarded as an antibacterial agent with unique biocompatibility. Decorating Au NPs on CeO_2 NPs (Au/CeO_2) would achieve a stronger bacterial inhibitory activity than CeO_2 NPs and pure Au NPs. Furthermore, after coculture bacteria with *Lactobacillus plantarum* (*L. plantarum*), *L. plantarum* and Au/CeO_2 NPs possibly act synergistically in inhibiting bacteria (Babu et al., 2014). In monoculture systems, the results showed that Au/CeO_2 NPs exhibited a broad-spectrum effect against four tested bacteria: *E. coli*, *Salmonella enteritidis* (*S. enteritidis*), *B. subtilis*, and *S. aureus*. Although ampicillin had a higher inhibiting effect against most bacteria, it failed to show an obvious antibacterial effect against *B. subtilis*. After coculture bacteria with *L. plantarum*, Au/CeO_2 NPs showed enhanced antibacterial activities against *S. aureus*, *B. subtilis*, and *S. enteritidis*. With different NPs or antibiotic doses increased, the bacterial concentration decreased at different degrees after incubation in a monoculture or coculture system. However, with the doses of Au NPs increased, it showed greater toxicity toward RAW 264.7 cells, whereas pure CeO_2 did not show any significant toxicity after 48 h (Babu et al., 2014).

Cerium Complexes

Cerium complexes with various ligands possessed different properties, such as antitumor and antimicrobial activities (Sang et al., 2017). Schiff base cerium complexes were reported to have interesting antibacterial activity (Sang et al., 2015, 2017). The MIC values of Schiff base cerium(IV) complex against *B. subtilis*, *S. aureus*, *E. coli*, and *Pseudomonas fluorescens* (*P. fluorescens*) ranged from 1.56 to 12.5 μg/ml. The inhibition activity of this cerium complex is weaker against *B. subtilis*, while stronger against other tested bacteria compared with penicillin (Sang et al., 2015). The Schiff base cerium(III) complex had stronger antibacterial activities against *B. subtilis*, *S. aureus*, *E. coli*, and *P. fluorescens* than the free Schiff base, and corresponding MIC values were in the range of 1.56 to 25 μg/ml (Sang et al., 2017). In another study, the Schiff base cerium(III) complex was reported to exhibit antibacterial activity with all MIC values of > 50 μg/ml against *S. aureus*, *K. pneumonia*, *E. coli*, *P. vulgaris*, and *Candida albicans* (*C. albicans*) (El-Shafiy and Shebl, 2018). The lipophilicity of the complex made it easier to penetrate into the lipid membrane and block the metal binding sites on enzymes of bacteria (Sang et al., 2015). In addition, the complex $NaCe(MoO_4)_2$ could act as antibiotic activity "modulators," increasing the activity of a specific antibiotic for a certain strain. When using sodium–cerium molybdate [$NaCe(MoO_4)_2$] alone, the MIC values were over 1,024 μg/ml, showing no antibacterial activity (Moura et al., 2019). $NaCe(MoO_4)_2$ synergistically modulated the activity of gentamicin against *S. aureus*, reducing the MIC values from 16 to 4 μg/ml, and norfloxacin against *E. coli*, reducing the MIC values from 8 to 3.17 μg/ml. $NaCe(MoO_4)_2$ showed antagonism when using norfloxacin against *S. aureus* and gentamicin and imipenem against *E. coli* together. This resulted from a chelation of the antibiotic by $NaCe(MoO_4)_2$ or a reverse reaction or binding to specific sites within the antibiotics, causing antibiotic spectrum reduction (Moura et al., 2019). The antimicrobial activities of element-doped CeO_2, antibacterial element incorporation/modification, and cerium complexes are summarized in **Table 2**.

CERIUM- AND CERIUM OXIDE-DOPED MATERIALS

Currently, semiconductor materials in nanoscale have drawn much attention because of their unique physical and chemical properties (Suresh, 2013). As such, metallic oxides, such as ZnO and TiO_2, are used as biocides or disinfecting agents due to their ability to induce the generation of ROS under UV light (Khan et al., 2015). When cerium and cerium oxide were doped into semiconducting nanomaterials, they functioned as inorganic disinfectants, with a higher antibacterial activity than pure semiconducting nanomaterials alone (Bomila et al., 2018). When cerium was doped into some scaffold materials such as HA, bioactive glass (BG), and metal organic frameworks (MOFs), these materials not only showed enhanced antibacterial properties but also achieved improved mechanical properties and biological properties (Gopi et al., 2014; Deliormanlı et al., 2016; Li et al., 2019a). The antimicrobial activities of cerium- and cerium oxide-doped materials are summarized in **Table 3**.

Cerium and Cerium Oxide Doping Into Metal Oxide

The antibacterial activity of ZnO resulted from the process of oxidative stress. Zn^{2+} ions could be absorbed by bacterial cells and inhibit the action of respiratory enzymes in cell membrane by interacting with them. Then they led to ROS formation, causing oxidative stress which led to irreversible damage to the bacterial cell (Mishra et al., 2017). The increased particle surface area, reduced band gap energy, and improved adsorption ability of the particle surfaces and dopant–ZnO interfaces contributed to better optical properties, high luminescence properties, and high photocatalytic activity in the doped semiconducting catalysts (Lee et al., 2016). Bomila et al. (2018) prepared pure and Ce-doped ZnO NPs and applied them as an antibacterial agent. With the increase in Ce dopants, the antibacterial effectiveness increased. The maximum Ce-doped ZnO NPs possessed higher antibacterial activity, which was closer to the antibacterial activity of positive control ampicillin. It was found that Ce-doped ZnO NPs had more effective antibacterial property than pure ZnO NPs, and both NPs had a selectively antibacterial activity toward Gram-negative bacteria. Flower-like ZnO had better photocatalytic activity than ZnO with other morphologies, which

TABLE 2 | The antimicrobial activities of element-doped CeO_2, antibacterial element incorporation/modification, and cerium complexes.

Design	Morphology	Form	Dose and Conditions		Pathogens	Antimicrobial/Inhibition Activity		References
						Parameters	Antimicrobial Efficiency	
Metal element-doped CeO_2	nanoparticles	Fe-doped CeO_2	N/A		*C. albicans*	MIC_{50}	0.12 μg/ml	Rahdar et al., 2019
						MIC_{90}	0.48 μg/ml	
	nanoparticles	Mn-doped CeO_2	20 μg/ml	Mn 3%, 5%, 7%, 9%	*E. coli*	ZOI	7, 7, 8, 8.5 mm	Atif et al., 2019
	nanoparticles	Co-doped CeO_2	1 mg/ml	Co 2%, 4%, 6%, 8%	*B. cereus*	ZOI	12, 16, 21, 27 mm	Khadar et al., 2019
					E. coli		13, 17, 21, 24 mm	
					S. aureus		13, 18, 20, 23 mm	
					S. typhi		15, 15, 19, 25 mm	
	nanoparticles	Sm-doped CeO_2	1 mg/ml	Sm 2%, 4%, 6%, 8%	*B. cereus*	ZOI	13, 18, 21, 25 mm	Balamurugan et al., 2019
					E. coli		13, 15, 18, 22 mm	
					S. aureus		13, 15, 18, 20 mm	
					S. typhi		12, 15, 19, 24 mm	
	nanorods nanocubes nanoparticles	Ag/CeO_2	2 wt.%, 120 min		*E. coli*	CFU reduction	4 log	Wang et al., 2014
Antibacterial element incorporation/ modification	nanostructure	Ag/CeO_2	50 μg/ml		*P. aeruginosa*	MIC	3.125 μg/ml	Negi et al., 2019
					S. aureus		6.25 μg/ml	
	nanocomposites	ceria/AgBr/Ag_3PO_4	dark		*E. coli*	CFU reduction	2 log	Eswar et al., 2015
		P-ceria/AgBr/Ag_3PO_4					> 2 log	
		ceria/AgBr/Ag_3PO_4	visible light				> 4 log	
		P-ceria/AgBr/Ag_3PO_4					4 log	
	nanocontainers	AgNP/CeO_2	90 mg/ml 100 μl		*E. coli*	ZOI MBC	2 mm 117 ± 6 mg/ml	Gagnon et al., 2016
	nanocontainers	$AgNO_3/CeO_2$	90 mg/ml			ZOI	4 mm	
			100 μl			MBC	93 ± 0.5 mg/ml	
	nanocontainers	AgNP/CeO_2/TiO_2	90 mg/ml		*E. coli*	ZOI	0.5 mm	Gagnon et al., 2016
	Spherical	Au/CeO_2	1,488 μM		*B. subtilis*	Inhibitory efficiency	69.6%	Babu et al., 2014
					S. enteritidis		45.7%	
					E coli		38.2%	
					S. aureus		24.2%	
Cerium complex		cerium(IV) complex	N/A		*B. subtilis*	MIC	3.12 μg/ml	Sang et al., 2015
					E. coli		12.5 μg/ml	
					P. fluorescens		6.25 μg/ml	
					S. aureus		1.56 μg/ml	
		cerium(III) complex	50 μg/ml		*B. subtilis*	MIC	1.56 μg/ml	Sang et al., 2017
					E. coli		25 μg/ml	
					P. fluorescens		12.5 μg/ml	
					S. aureus		3.12 μg/ml	
		cerium(III) complex	N/A		*E. coli*	MIC	> 50 μg/ml	El-Shafiy and Shebl, 2018
					K. pneumonia			
					P. vulgaris			
					S. aureus			
					C. albicans			
		$NaCe(MoO_4)_2$	1,024 mg/ml		*E. coli*	MIC	≥ 1,024 μg/ml	Moura et al., 2019
					P. aeruginosa			
					S. aureus			
		$NaCe(MoO_4)_2$ + norfloxacin			*E. coli*	MIC	Synergism (3.17 μg/ml)	

(Continued)

TABLE 2 | Continued

Design	Morphology	Form	Dose and Conditions	Pathogens	Antimicrobial/Inhibition Activity		References
					Parameters	Antimicrobial Efficiency	
				P. aeruginosa		No significant difference	
				S. aureus		Antagonism	
		$NaCe(MoO_4)_2$ + gentamicin		*E. coli*	MIC	Antagonism	
				P. aeruginosa		No significant difference	
				S. aureus		Synergism (4 μg/ml)	
		$NaCe(MoO_4)_2$ + imipenem		*E. coli*	MIC	Antagonism	
				P. aeruginosa		No significant difference	
				S. aureus		No significant difference	

B. cereus, Bacillus cereus; B. subtilis, Bacillus subtilis; C. albicans, Candida albicans; E. coli, Escherichia coli; K. pneumoniae, Klebsiella pneumoniae; MBC, minimum bactericidal concentration; MIC, minimum inhibitory concentration; MIC_{50}, half minimum inhibitory concentration; MIC_{90}, 90% minimum inhibitory concentration; P-ceria, synthesis of ceria PEG-assisted sonochemical method; P. aeruginosa, Pseudomonas aeruginosa; P. fluorescens, Pseudomonas fluorescens; P. vulgaris, Proteus vulgaris; S. aureus, Staphylococcus aureus; S. enteritidis, Salmonella enteritidis; S. typhi, Salmonella typhi; ZOI, zone of inhibition.

is closely related to antimicrobial activity (Chelouche et al., 2014). With the adding of cerium ion doping, the band gap of ZnO crystallites decreased, which could take advantage of visible-light irradiation and hence produce more ROS (Hui et al., 2016). The 0.8% Ce-doped flower-shaped ZnO crystallites enhanced antimicrobial activity against *C. albicans* (75%) and *Aspergillus flavus* (80%) under visible-light sources than pure ZnO crystals (Hui et al., 2016). Reduced graphene oxide (rGO) could improve the adsorption of water and oxygen molecules and react with electron and hole pairs. This process is beneficial to production of excess ROS and direct contact with bacteria, which promote ZnO to form cavities on the bacterial cell. Ce could suppress the electron trapping effect and promote ROS generation. The Ce-doped ZnO/rGO (Ce/ZnO/rGO) with impaired flower-like morphology showed enhanced an antibacterial effect against both Gram-positive *B. subtilis* and Gram-negative *Vibrio harveyi* (Vanitha et al., 2018).

TiO_2 with low toxicity, good biocompatibility, and high bactericidal and sterilizing effects has become one of the most promising antimicrobial materials (Qi et al., 2019a). However, its wide band gap made it function only in UV irradiation which might cause skin damage and disorders and restricted tissue penetration, seriously influencing the application of TiO_2 in the antibacterial field (Qi et al., 2019a). Doping non-metal ions or metal ions could broaden the visible-light response, which would make it possible for TiO_2 nanomaterials to have a photocatalytic effect under visible-light irradiation. The calcination temperature during the synthesis may affect the antibacterial effect. Wang et al. exchanged ions into the materials and prepared single-Zn-ion-doped TiO_2 (Zn-TiO_2) and double-ion-doped TiO_2 (Zn/Ce-TiO_2, Zn/Y-TiO_2, and Zn/B-TiO_2) at different calcination temperatures. The results showed that only Zn-TiO_2 nanomaterials calcinated at 500°C had a bactericidal effect due to a large surface area. After doping with Ce, Y, or B ions, the bactericidal activities of the Zn-TiO_2 materials are significantly improved at different calcination temperatures (Wang et al., 2017). In their next experiment, TiO_2 materials co-doped with B and Ce ions (B/Ce–TiO_2) with different calcination temperatures were prepared, and all materials had a large ZOI, suggesting that the materials have excellent antimicrobial activities (Wang et al., 2018). Besides the antibacterial effect of Ce, B_2O_3 was found in the materials and is dissolved in water to produce metabolic acid and boric acid. Boric acid had an inhibitory effect on all kinds of bacteria and fungi. CeO_2-doped TiO_2 nanocomposites were found to have no inhibitory effect on bacterial growth without UV light. When exposed to UV light, nanocomposites showed inhibition in different degrees. Gram-positive strains were more susceptible than Gram-negative strains. As doping concentrations of TiO_2 increased, the ZOI of both pathogens increased (Kasinathan et al., 2016). Similarly, Moongraksathum and Chen (2018) synthesized anatase TiO_2 co-doped with Ag and CeO_2 (Ag/CeO_2-TiO_2). Remarkably, they took full advantage of the photocatalytic properties of TiO_2 and CeO_2, and the addition of silver could broaden the bactericidal activity of photocatalytic composite materials. After 30 min of illumination with UVA (λ = 365 nm) radiation, the bactericidal efficiency of Ag/CeO_2-TiO_2 coating could reach more than 99.99% against both *E. coli* and *S. aureus* (Moongraksathum and Chen, 2018). The order of antibacterial effectiveness of tested materials against both *E. coli* and *S. aureus* was Ag/CeO_2-TiO_2 > Ag/TiO_2 > CeO_2-TiO_2 > TiO_2.

Similar to ZnO and TiO_2, ZrO_2 is also a significant semiconductor material in the biomedical field. ZrO_2 is an n-type semiconductor with a broad strap gap, and when it is doped with rare-earth metals, it exhibits an outstanding structural stability, high thermal conductivity, and irradiation stability. Ce doping could enhance the ROS generation capability of ZrO_2 NPs. The antibacterial property of Ce-doped ZrO_2 NPs was found

TABLE 3 | The antimicrobial activities of cerium- and cerium oxide-doped materials.

Design	Morphology	Form	Dose and Conditions	Pathogens	Antimicrobial/Inhibition Activity		References
					Parameters	Antimicrobial Efficiency	
Ce- and CeO_2-doped materials	spherical shaped	Ce-doped ZnO	molar concentration of Ce 0.03–0.07	*P. mirabilis*	ZOI	16.33 ± 0.7 to 18.66 ± 0.7 mm	Bomila et al., 2018
				S. typhi		16.66 ± 0.2 to 27.33 ± 0.7 mm	
				S. aureus		NA to 7.33 ± 0.2 mm	
				B. subtilis		NA to 7.66 ± 0.7 mm	
	slower shaped	Ce-doped ZnO	[Ce]/[Zn] 0.4%, 0.6%, 0.8%, 1.0%	*A. flavus*	Inhibition rates	66%, 77%, 78%, 80%	Hui et al., 2016
			[Ce]/[Zn] 0.4%, 0.6%, 0.8%, 1.0%	*C. albicans*		58%, 72%, 75%, 73%	
	impaired flower shaped	Ce/ZnO/rGO	N/A	*B. subtilis*	ZOI	20 mm	Vanitha et al., 2018
				V. harveyi		12.5 mm	
	round aggregation	Zn/Ce-TiO_2	visible light	*E. coli*	KR	1, 3, 1, 0	Wang et al., 2017
			calcination temperature				
			500°C, 600°C, 700°C, 800°C				
	nanocomposites	B/Ce–TiO_2	visible light	*E. coli*	KR	0, 2, 2, 1.5	Wang et al., 2018
			calcination temperature				
			500°C, 600°C, 700°C, 800°C				
			500°C, 600°C, 700°C, 800°C	*S. aureus*	KR	0, 1.5, > 4, 1.4	
	nanocomposites	CeO_2-doped TiO_2	25, 50, 75, 100 μg/ml	*E. coli*	ZOI	2.2, 3.2, 4.1, 4.5 mm	Kasinathan et al., 2016
				S. aureus		2.5, 5, 4.9, 5.2 mm	
				P. vulgaris		3.4, 8, 10.2, 12.1 mm	
				S. pneumonia		6, 11, 12.5, 15.5 mm	
	films	Ag/CeO_2-TiO_2	UVA 30 min	*E. coli*	Antibacterial effectiveness (%)	> 99.99	Moongraksathum and Chen, 2018
				S. aureus		> 99.99	
			UVA 60 min	*E. coli*		> 99.99	
				S. aureus		> 99.99	
	nanoparticles	Ce-doped ZrO_2	50 μg/ml	*B. subtilis*	ZOI	15 mm	Mekala et al., 2018
				S. aureus		16 mm	
				K. pneumonia		15 mm	
				P. aeruginosa		11 mm	
Ce- and CeO_2-doped materials	nanoparticles	Ce-doped NiO	1 wt.% Ce	*K. pneumoniae*	ZOI (mm)	–, > 100, > 100	Muthukumaran et al., 2016
				S. typhi		9, 80, 90	
				P. aeruginosa		10, 60, 70	
				B. cereus		10, 60, 60	
				B. subtilis	MIC (μg/ml)	15, 20, 20	
				S. aureus		14,20, 30	
			9 wt.% Ce	*K. pneumoniae*		–, > 100, > 100	
				S. typhi		12, 40, 50	
				P. aeruginosa	MBC (μg/ml)	10, 60, 70	
				B. cereus		10, 40, 40	
				B. subtilis		25, 20, 30	
				S. aureus		13, 30, 30	

(Continued)

TABLE 3 | Continued

Design	Morphology	Form	Dose and Conditions	Pathogens	Antimicrobial/Inhibition Activity		References
					Parameters	**Antimicrobial Efficiency**	
	nanoparticles	$CoCe_xFe_{2-x}O_4$	$x = 0.0, 0.1, 0.3, 0.5$	*S. aureus*	ZOI	12, 14, 16, 19 mm	Elayakumar et al., 2019a
				K. pneumoniae		14, 14, 16, 17 mm	
	nanoparticles	$CuCe_xFe_{2-x}O_4$	$x = 0.2, 0.3, 0.4, 0.5$	*S. aureus*	ZOI	20, 21, 19, 18 mm	Elayakumar et al., 2019b
				K. pneumoniae		21, 23, 25, 27 mm	
	nanoparticles	ZIF-8 : Ce	30 µg/ml	*P. gingivalis*	CFU reduction	> 2 log, >1 log, 1.5 log	Li et al., 2019a
		1%, 5%, 10%		*F. nucleatum*		> 0.5 log, < 0.5 log, < 0.5 log	
	Composite	GR-HA_Ce	90 min	*S. aureus*	Bacterial adhesion reduction	18.2%	Morais et al., 2015
				S. epidermidis		27.3%	
				P. aeruginosa		-14.6%	
	nanoparticles	Ca/Sr/Ce-HA	25, 50, 75, 100, 125 µl	*E. coli*	ZOI	11, 12, 13, 14, 15 mm	Gopi et al., 2014
			0.1 M	*S. aureus*		10, 11, 12, 13, 14 mm	
	powders	Ce/Si-co-doped HAP	Ce/Si-HAP@1, 3, 5 wt%	*E. coli*	Bactericidal rate	82.1%, 88.7%, 90.4%	Priyadarshini and Vijayalakshmi, 2018
				S. aureus		69.6%, 80.3%, 88.8%	
				P. aeruginosa		41.4%, 61.7%, 75.8%	
				B. subtilis		31.3%, 46.2%, 66.3%	
	nanopowder	HA-Ce-0/HA-Ce-10	0, 9.5%, 19.4%, 24.7% Ce	*E. coli*	Microbial inhibition	16.43%, 31.38%	Ciobanu et al., 2015
						53.33%, 93.75%	
		HA-Ce-20/HA-Ce-25		*S. aureus*		18.48%, 29.01%	
						34.03%, 60.61%	
	composite coating	HA-Ce-Ti	N/A	*E. coli*	Bactericidal ratio	92.61%	Ciobanu and Harja, 2019
				S. aureus		73.59%	
Ce- and CeO_2-doped materials	scaffolds	Ce^{3+}-doped fluorapatites	25 µg/ml	*E. coli*	IC_{50}	107 ± 7.1 µg/ml	Anastasiou et al., 2019
				S. aureus		135 ± 9.3 µg/ml	
			50 µg/ml	*B. subtilis*		133 ± 8.1 µg/ml	
			100 µg/ml	*B. cereus*		165 ± 11.5 µg/ml	
	composites	BG containing 5 mol% and 10 mol% Ce	10 mg/ml	*E. coli*	Survival rate	Nearly 0%	Goh et al., 2014
	scaffolds	CeBG	N/A	*E. coli*	ZOI	No	Deliormanlı et al., 2016
				S. aureus			
	composite nanofibers	BG doped with 5 and 10 mol% Ce	N/A	*E. coli*	ZOI	No	Goh et al., 2016

A. flavus, Aspergillus flavus; B. cereus, Bacillus cereus; BG, bioactive glasses; B. subtilis, Bacillus subtilis; C. albicans, Candida albicans; E. coli, Escherichia coli; F. nucleatum, Fusobacterium nucleatum; HA, HAP, hydroxyapatite; IC_{50}, 50% inhibiting concentration; KR = log(Nsc/Ns), where Nsc is the total amount of microorganism colonies in the control tube (a sterile 0.8 wt.% saline water without material) and Ns is the total amount of microorganism colonies. If KR ≤ 0, the system has no antimicrobial effect, while KR > 0 indicates antimicrobial effect. The higher the value of KR, the more evident is the antimicrobial effect. MBC, minimum bactericidal concentration; MIC, minimum inhibitory concentration; P. aeruginosa, Pseudomonas aeruginosa; P. gingivalis, Porphyromonas gingivalis; P. mirabilis, Proteus mirabilis; P. vulgaris, Proteus vulgaris; rGO, reduced graphene oxide; S. aureus, Staphylococcus aureus; S. epidermidis, Staphylococcus epidermidis; S. typhi, Salmonella typhi; UVA, ultraviolet radiation A; V. harveyi, Vibrio harveyi; ZIF-8, zeolitic imidazole framework-8; ZOI, zone of inhibition.

more efficient in Gram-positive bacteria than in Gram-negative bacteria. The ZOI values of Ce-doped ZrO_2 against *B. subtilis* and *S. aureus* were 15 and 16 mm, respectively, while those against *Klebsiella pneumoniae* (*K. pneumoniae*) and *P. aeruginosa* were 15 and 11 mm, respectively (Mekala et al., 2018).

The Ce-doped nickel oxide (Ce-doped NiO) nanomaterial also achieved excellent antibacterial activity against *K. pneumoniae*, *S. typhi*, *P. aeruginosa*, *B. cereus*, *B. subtilis*, and *S. aureus* (Muthukumaran et al., 2016). Among the samples of Ce-doped NiO with different weight percentages (pure and 1, 3, 5, 7, and 9 wt.%), 5 wt.% Ce-doped NiO, which showed the maximal catalytic peak current during the anodic scan, got the best antibacterial activity against all tested bacteria with the MIC and MBC (**Figure 4**). Elayakumar et al. (2019a,b) prepared different concentrations of Ce-ion-doped magnetic spinel ferrite NPs ($MCe_xFe_{2-x}O_4$, where M denotes divalent metal ions Co and Cu and x = 0.0, 0.1, 0.2, 0.3, 0.4, and 0.5). The results indicated that the antibacterial activity depended on concentration of Ce^{3+}. Higher concentrations of Ce^{3+}-doped $MCe_xFe_{2-x}O_4$ spinel matrix influenced higher antibacterial activity with a larger ZOI than that of lower concentrations of Ce^{3+}-doped $MCe_xFe_{2-x}O_4$ nanopowders.

Besides, MOFs, as effective and promising therapeutic nanomaterials constructed by bridging metal ions with organic linkers, have sparked increasing interest in the field of antibacterial applications, as they have the ability of reserving metal ions and keeping continuous ion release in order to attain bacteriostatic and bactericidal effects (Wyszogrodzka et al., 2016; Zhang et al., 2018; Wang et al., 2019). Recently, the novel multifunctional NPs (ZIF-8 : Ce) were synthesized by doping Ce into the zeolitic imidazole framework-8 (ZIF-8). The materials possessed antibacterial capabilities against two periodontal pathogens *Porphyromonas gingivalis* (*P. gingivalis*) and *Fusobacterium nucleatum* (*F. nucleatum*) as well as anti-inflammatory capabilities (Li et al., 2019a). As shown in **Figure 5**, ZIF-8 and ZIF-8 : Ce1% NPs obtained about 2 log CFU reduction against *F. nucleatum* and *P. gingivalis*. The antibacterial effect was decreased with the increase of Ce substituting quantity. The antimicrobial activity of ZIF-8 was attributed to Zn, Ce, and the disruption of liposome from imidazole. In addition, Ce doping endowed ZIF-8 NPs with superoxide dismutase (SOD) and catalase (CAT) enzyme mimic activities for ROS scavenging, which could be beneficial for eliminating the inevitable inflammatory response during antibacterial application (Li et al., 2019a).

Cerium and Cerium Oxide Doping Into Grafting Scaffold

Hydroxyapatite, an essential macroporous inorganic material, has the same component as dentine, enamel, and bones and has several excellent properties. Therefore, HA has been widely studied in tissue engineering as a grafting scaffold and applied in the biomedical field such as dentistry, maxillofacial reconstruction, and implant coatings (Phatai et al., 2018). However, admittedly, pure HA has several disadvantages such as being brittle and weak in intensity and adhesion, dissolution rate, and antibacterial capacity (Phatai et al., 2018). The introduction of Ce^{3+} could improve mechanical properties, antibacterial activity, and cell adhesion and proliferation of HA-based composites (Gopi et al., 2014; Morais et al., 2015). Because the electronegativity and radius of Ce^{3+} are very close to those of Ca^{2+}, Ce^{3+} can replace Ca^{2+} within the HA lattice. Ce-doped HA can stimulate metabolic activity in organisms and improve its antibacterial property (Yuan et al., 2016). Ce-doped glass-reinforced HA composite (GR-HA_Ce) was reported to have the ability to induce osteoblast adhesion and proliferation and enhance the expression of osteoblastic-related genes (Morais et al., 2015). Compared to the pure HA and GR-HA_control, the GR-HA_Ce surface had a significant decrease of the bacterial adhesion for *S. aureus* and *S. epidermidis* at 30, 60, and 90 min of incubation. However, for *P. aeruginosa*, it showed the opposite results in that the reduction of bacterial adhesion in the GR-HA control performs better than in the GR-HA_Ce. Ca/Sr/Ce–HA NPs were found to have an enhanced antibacterial effect after Sr^{2+} and Ce^{3+} co-substitution. The crystallinity decreased, and the surface area of the as-synthesized NPs increased through forming bonds with the microorganisms, causing cell death (Gopi et al., 2014). Ce ions acted as an antibacterial agent, and Si^{4+} ions played a crucial role in the development of apatite nuclei (Priyadarshini and Vijayalakshmi, 2018). Priyadarshini and Vijayalakshmi synthesized 1.25% of Ce along with 1, 3, and 5% of Si co-doped HA. The CFU result showed that the developed 1–5% of Si-co-doped Ce-HA had excellent bacterial inhibition and that the 5% of Si-co-doped Ce-HA got the maximum antibacterial activity. The order of inhibition efficiency against pathogens was *E. coli* > *S. aureus* > *P. aeruginosa* > *B. subtilis* (Priyadarshini and Vijayalakshmi, 2018). In addition, Ciobanu et al. (2015) prepared new Ce^{4+}-substituted HA nanopowders with a more effective killing efficiency against *E. coli* than against *S. aureus*. As the Ce concentration in HA increased to 25%, the microbial inhibition against *E. coli* and *S. aureus* came to the maximum, which was 93.75% and 60.61%, respectively, since more cerium ions were released to inhibit bacteria by the improved solubility of Ce^{4+}-HA. HA coatings were also widely studied and used since they could promote the osseointegration between metal implants and bone, causing no immune rejection. It was reported that cerium-doped HA/collagen coatings could kill 92.61% of *E. coli* and 73.59% of *S. aureus* after 24 h of incubation, whereas a pure HA layer did not show antibacterial properties. As mentioned above, the decreased crystallinity caused increased solubility, resulting in more cerium ions released, which make contact with the bacterial membrane and eventually cause bacterial death (Ciobanu and Harja, 2019). In addition, the chitosan scaffold embedded with Ce^{3+}-doped fluorapatite was developed as a scaffold material for preventing bacterial infections in orthopedics and regenerative dentistry. The results have shown that both undoped and Ce^{3+}-doped fluorapatites present better antibacterial effect than the Sr^{2+}-doped ones. Importantly, high osteoconductivity leading to the differentiation of the dental pulp stem cells into osteoblasts was detected in Ce^{3+}- and Sr^{2+}-doped fluorapatites (Anastasiou et al., 2019).

Bioactive glass is also one of the promising materials applied in bone-related biomedical fields for bone regeneration,

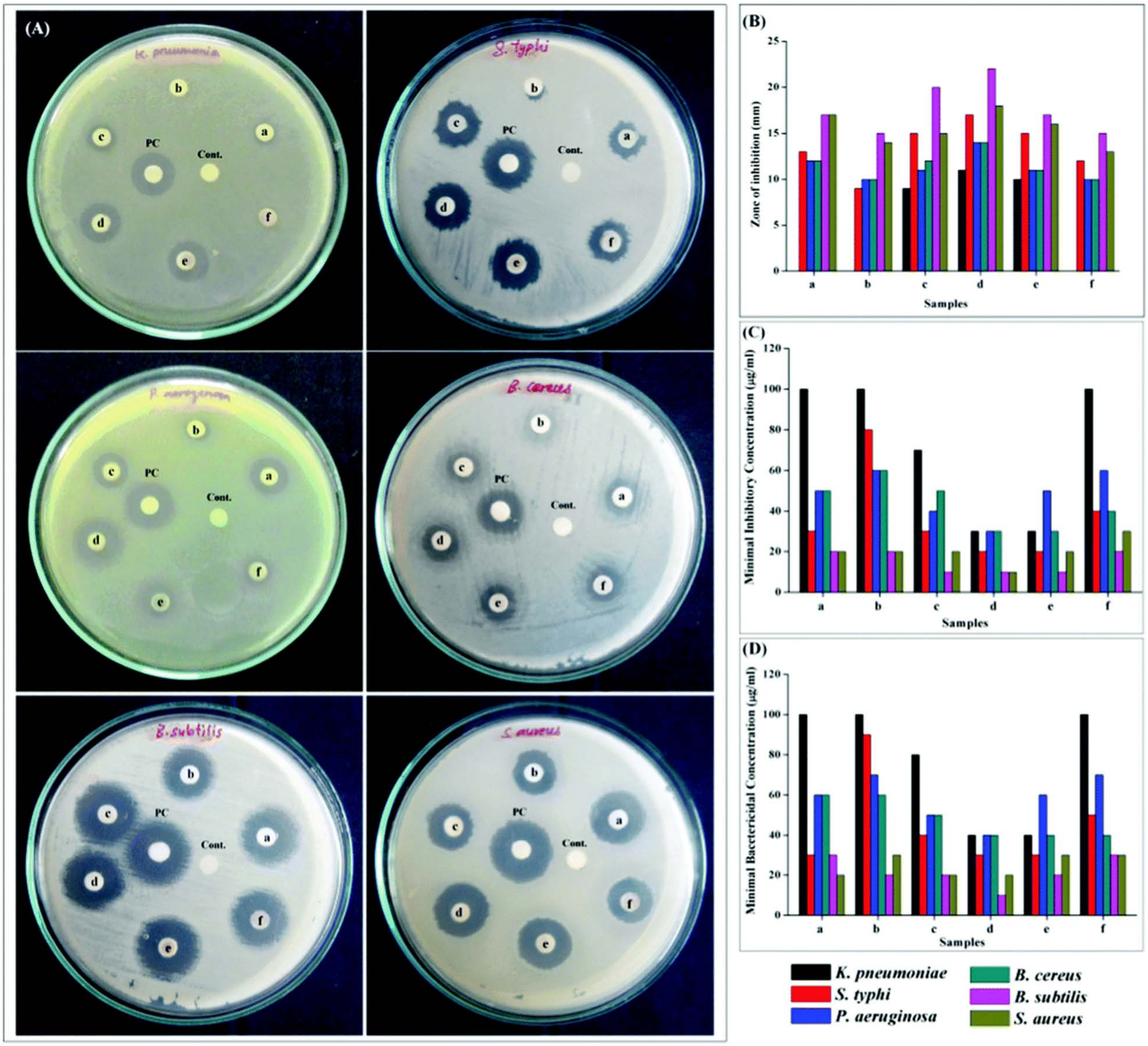

FIGURE 4 | Antibacterial activity using **(A)** disk diffusion assay for NiO and 1, 3, 5, 7, and 9 wt.% Ce-doped NiO (samples a–f), PC (positive control), and C (negative control). **(B)** Zone of inhibition, **(C)** MIC, and **(D)** MBC analyses. Reprinted with permission from Muthukumaran et al. (2016), copyright 2016 Royal Society of Chemistry.

vascularization stimulation, wound healing, monolithic medical devices, oral care for treatment of hypersensitivity, and implant coatings (Jones, 2015). It was reported that high concentration of BG could kill various microorganisms because the process of its dissolution could release cations and lead to pH rise (Stoor et al., 1998). However, the low concentration of BG showed no antibacterial effect, and when it is doped with various antibacterial ions, such as Ce^{3+}, its antibacterial property could be improved (Goh et al., 2014). In a previous study, the antibacterial activity of BG doping with 1, 5, and 10 mol% Ce was investigated by the quantitative viable count method. As a result, the BG containing 5 and 10 mol% Ce showed a significant antibacterial effect on *E. coli*, but there were no significant differences between the antibacterial property of BG containing 5 and 10 mol% Ce (Goh et al., 2014). Deliormanlı et al. (2016) prepared cerium-, gallium-, and vanadium-doped porous scaffolds of borate BG and studied the soft tissue ingrowth and angiogenesis in the materials. After subcutaneous implantation in rats for 4 weeks, an increase was observed in angiogenesis for cerium-doped scaffolds (CeBG), whereas a decrease was obtained in angiogenesis for the other two types of scaffolds (Deliormanlı et al., 2016). However, all of the scaffolds prepared in this study did not exhibit any antibacterial activity toward *E. coli* and *S. aureus* by a zone inhibition method. Electrospun polylactic acid (PLA)/chitosan nanofibers coated with cerium-, copper-, or silver-doped bioactive glasses

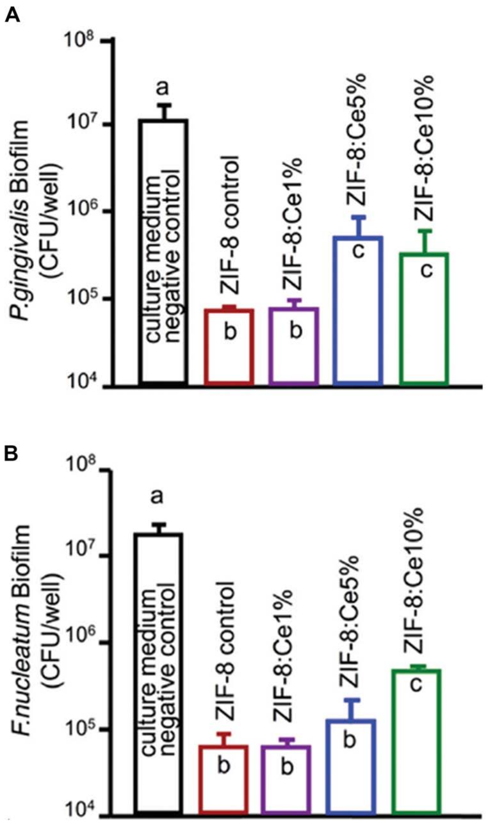

FIGURE 5 | Colony-forming unit counts of 4-day biofilms of **(A)** *P. gingivalis* and **(B)** *F. nucleatum*. Note the log scale for the *y*-axis. Reprinted with permission from Li et al. (2019b), copyright 2019 Royal Society of Chemistry.

(CeBG/CuBG/AgBG) were prepared, and antibacterial activities against *E. coli* were measured by the disk diffusion method (Goh et al., 2016). However, in this study, CeBG- and CuBG-decorated PLA/chitosan nanofibers showed no ZOI against the bacteria. The authors indicated that the disk diffusion method is affected by the diffusion rate, and therefore, it was suggested to use other methods such as the quantitative viable count method to investigate their antibacterial activities.

In addition to doping, Ce and CeO_2 could also blend with other materials without any chemical bond which would take the advantages of each component and modify the original material. For example, HA with 5 wt.% CeO_2 NPs and 2.5 wt.% Ag NPs (HA-5C-2.5Ag) had enhanced mechanical properties and antibacterial properties. In addition, the materials showed advantages of ROS scavenging, rapid healing promotion, and cell growth improvement (Pandey et al., 2018a).

Polymer Matrixes Containing Cerium and Cerium Oxide

Chitosan is a natural non-toxic biopolymer with many advantages such as low toxicity, high susceptibility to biodegradation, mucoadhesive nature, capacity to enhance drug permeability and absorption, and antimicrobial and antifungal activity (Qi et al., 2004). Therefore, Ce^{3+} ions and chitosan with alginate films (Ce-Chi films) could act as wound dressing materials, showing an increasing reduction in CFU counts of *E. coli* and *S. aureus* during the 3-h exposure period (Kaygusuz et al., 2017). It was also reported that NPs with Ce and CeO_2 blended with chitosan (hybrid Chi-CeO_2) had enhanced antimicrobial activity. The maximum ZOI values were around 11 and 8 mm against *E. coli* and *B. subtilis*, respectively. In addition, significant morphological changes against *E. coli* and *B. subtilis* could be observed from the SEM images (Senthilkumar et al., 2017).

In addition, some materials made up of polymer matrixes containing cerium and cerium oxide were found to have antibacterial efficiency. Ureasil polyethylene oxide (U-PEO) was loaded with a combination of Ce and Ag salts. Among various materials, the U-PEO : Ce0Ag1 hybrid showed the best antibacterial efficiency, and the U-PEO : Ce0.90Ag0.10 hybrid had the best compromise between antibacterial efficiency, transparency, and photostability (Truffault et al., 2016). A mesoporous hybrid nanocomposite (CeO_2@AlOOH/PEI) prepared by CeO_2 NPs, boehmite (AlOOH), and polyethylene imine (PEI) showed excellent antibacterial efficiency toward *E. coli*, *K. pneumoniae*, and *S. aureus* (Shuhailath et al., 2016). However, these polymers had no biodegradation, which might limit their clinical applications.

CERIUM- AND CERIUM OXIDE-DECORATED MATERIALS

Titanium and its alloys have been widely used for orthopedic and dental implants because of their high rate of success. However, complications such as biomaterial-related infection often occurred and led to long-term hospital stay, higher morbidity, and mortality (Zhao et al., 2015). Therefore, people began to pay attention to the study of antibacterial TiO_2 coating. TiO_2 coatings doped with different percentages of CeO_2 (5%, 10%, and 20%) were deposited on titanium by an atmospheric plasma spraying technique (Zhao et al., 2015). The results showed that all coatings had micro-sized rough surfaces and a better interfacial bonding of TiO_2 and CeO_2/TiO_2 coatings. The 10% CeO_2/TiO_2 coating displayed the highest effectiveness in inhibiting *S. aureus* with 98% sterilization rates. Recently, CeO_2 with different nanostructures (nanorod, nanocube, and nano-octahedra) were synthesized via hydrothermal procedures and coated onto the surface of titanium to mimic dental implant coatings for antibacterial and anti-inflammatory purposes (Li et al., 2019b). In this paper, among the three shapes of nano-CeO_2, the octahedra-CeO_2 exhibited the highest Ce^{3+} value and the strongest ROS scavenging capacity and therefore had the strongest inhibition against early adhesion of peri-implantitis-related pathogens, which are shown in **Figure 6**, and the best anti-inflammatory effect. The better properties of octahedra-CeO_2 mainly attributed to its small size and the unique octahedral structure exposing more crystalline planes.

Bacterial biofilm is one of the primary causes of antibiotic resistance and immune response resistance, which led to

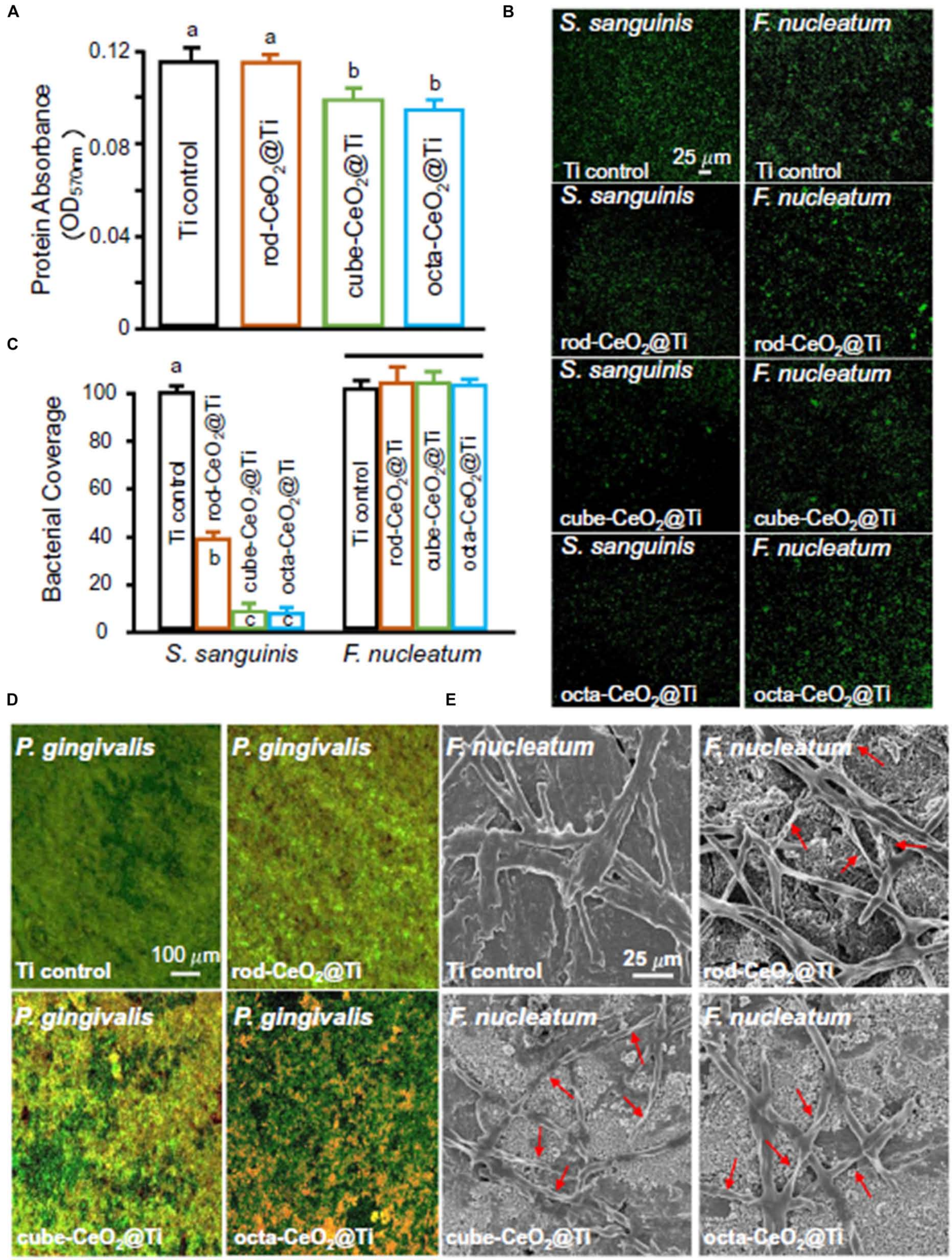

FIGURE 6 | The antibacterial properties of three different types of CeO_2-modified Ti. **(A)** Protein adsorption onto different surfaces ($n = 6$; mean ± SD). Dissimilar letters indicate values that are significantly different from each other ($p < 0.05$). **(B,C)** CLSM images and area cover fractions of *S. sanguinis* and *F. nucleatum* early colonization onto Ti at 4 h ($n = 6$; mean ± SD). Ti control was equal to 100%, and other groups were a percentage of Ti control. The solid line indicates that there

(Continued)

FIGURE 6 | Continued
are no significant differences between each group ($p > 0.1$). **(D)** Representative live/dead images of 4-day biofilms of *P. gingivalis* on Ti with different surfaces. *S. sanguinis* and *F. nucleatum* had similar live/dead images as *P. gingivalis*. Live bacteria were stained green. Dead bacteria were stained red. When live and dead bacteria were in close proximity or on top of each other, the staining had yellow or orange colors. **(E)** SEM images show the obvious *F. nucleatum* bactericidal effect of CeO_2-functionalized Ti disks. The position indicated by the red arrow is the breakdown and structures of dead bacteria. Reprinted with permission from Li et al. (2019b), copyright 2019 Elsevier.

persistent infections and increase in the difficulties for clinical treatment (Wu et al., 2015; Liu et al., 2019). Cerium- or cerium oxide-decorated materials could effectively inhibit the formation of biofilm, disturb the established biofilm, and eliminate the biofilm (Chen et al., 2016; Liu et al., 2019; Qiu et al., 2019). Herein, CeO_2-decorated porphyrin-based MOFs were designed to inhibit biofilm formation (Qiu et al., 2019). A 40% reduction in biomass was found in 50 μg/ml of the MOF@CeO_2 NP group, and after light irradiation for 5 min, the inhibition of the formation of biofilm is over 70%. When the concentration of MOF@CeO_2 increased to 200 μg/ml, the inhibition rate was over 90%. The results were attributed to the synergic effect of extracellular adenosine triphosphate (eATP) deprivation and ROS generation. In the subcutaneous abscess model, only the group treated with MOF@CeO_2 NPs and light irradiation was found to have no evident abscess after 5 days, and there were almost no viable counts of bacteria observed by using the spread plate method. Besides, hematoxylin and eosin (H&E) staining sections of the group treated with MOF@CeO_2 NPs and light irradiation showed a small number of inflammatory cells, while a large number of aggregated inflammatory cells were observed in the control group. In another study, $MOF_{-2.5Au-Ce}$, a series of MOF/Ce-based nanozymes with dual enzyme-mimetic activities including deoxyribonuclease (DNase) and peroxidase mimetic activities, was designed and, in the presence of H_2O_2, had ability to penetrate the biofilms, intensively inhibit bacterial biofilm formation *in vitro*, and treat subcutaneous abscess *in vivo* (Liu et al., 2019; **Figure 7**). The cerium(IV) complexes could hydrolyze eDNA and disrupt established biofilms; meanwhile, in the presence of H_2O_2, the MOF could kill bacteria exposed in dispersed biofilms. $MOF_{-2.5Au-Ce}$ applied alone could disperse biofilms moderately without killing bacteria. When treating with $MOF_{-2.5Au-Ce}$ and H_2O_2, most of the biofilms were destroyed. In the subcutaneous abscess mice model, the group treated with $MOF_{-2.5Au-Ce}$ + H_2O_2 showed good wound healing, and a scab was forming after 7 days, while the group treated with $MOF_{-2.5Au-Ce}$ alone and other groups still had suppuration and inflammation in the wound sites. Sections of histological evaluation of the abscess showed a dramatic reduction of inflammatory cells and intact epidermal layer in the $MOF_{-2.5Au-Ce}$ group. In addition, Chen et al. (2016) confined AuNPs with multiple cerium(IV) complexes on the surface of colloidal magnetic Fe_3O_4/SiO_2 core/shell particles to combat bacterial biofilms. Bacterial adhesion was strongly reduced, and biofilm formation was prevented over 120 h by the DNase-mimetic artificial enzyme (DMAE) via degrading the eDNA. Preformed biofilms of varying ages were effectively dispersed; meanwhile, the DMAE enhanced the antibacterial activity against the biofilm of antibiotics.

ZrP is a zirconium bis-(monohydrogen orthophosphate) monohydrate $[Zr(HPO_4)_2{\cdot}H_2O]$, serving as ion exchangers, catalysts, and carriers of intercalation (Cai et al., 2012). Layered ZrP-based antimicrobials were synthesized and modified with a series of Zn^{2+} or/and Ce^{3+}, denoted as Zn/ZrP, Ce/ZrP, and Zn-Ce/ZrP (Cai et al., 2012). Zn^{2+} intercalated into the interlayer of ZrP, while Ce^{3+} was adsorbed on the surface of ZrP through hydrogen bonds. In this study, Zn-Ce/ZrP achieved the strongest sterilization effect, due to the synergistic antibacterial effect of Zn^{2+} and Ce^{3+}. The two cations could target the cell membranes, causing huge damage to bacteria, and interact with each other to produce more hydroxylic free radicals to induce oxidative stress. Shu et al. loaded CeO_2 and ZnO NPs onto the surface of halloysite nanotubes (HNTs), forming CeO_2-ZnO/HNTs ternary nanocomposites (Shu et al., 2017). The cell viability of *E. coli* treated with pure ZnO, ZnO/HNTs, and CeO_2-ZnO/HNTs was 18%, 12%, and 8%, respectively. The modification of CeO_2 could slow down the recombination of electron–hole pairs and narrow the energy gap of ZnO NPs. The addition of HNTs could hinder the agglomeration of ZnO NPs and promote nanocomposites to react with the bacterial membranes. In another study, *N*,*N*,*N*-trimethyl chitosan (TMC) with CeO_2 NPs (TMC-CeO_2), a biopolymer with a positive charge, exhibited antibacterial behavior and protected normal cells from oxidation (Mohammad et al., 2017). From the results, the ZOI values of TMC-CeO_2 against *S. aureus* and *E. coli* at an MIC of 100 mg/ml were similar to ZOI values of pure CeO_2 at an MIC of 200 mg/ml. The contribution of effects was due to enhanced interactions between the composite and the bacterial cell.

CeO_2 BLEND WITH OTHER NANOMATERIALS

The CeO_2-GO hybrid nanocomposites showed an excellent synergic effect in increasing photocatalytic activity due to interface staggered band alignments existing between the CeO_2 surfaces and GO (Kashinath et al., 2019). It was reported that enhanced photocatalytic activity showed a fivefold better performance, and therefore, it showed increasing antibacterial activity. The CeO_2-GO hybrid nanocomposites showed highly controlled growth of bacteria in both *S. aureus* and *P. aeruginosa*. When compared with pure CeO_2 and GO, CeO_2-GO hybrid nanocomposites had smaller values of MICs and MBCs. Based on this, CeO_2- and peppermint oil (PM oil)-embedded polyethylene oxide/GO (PEO/GO) nanofibrous mats were developed as antibacterial wound dressings (Bharathi and Stalin, 2019). CeO_2-PM oil-PEO/GO nanofibrous mats

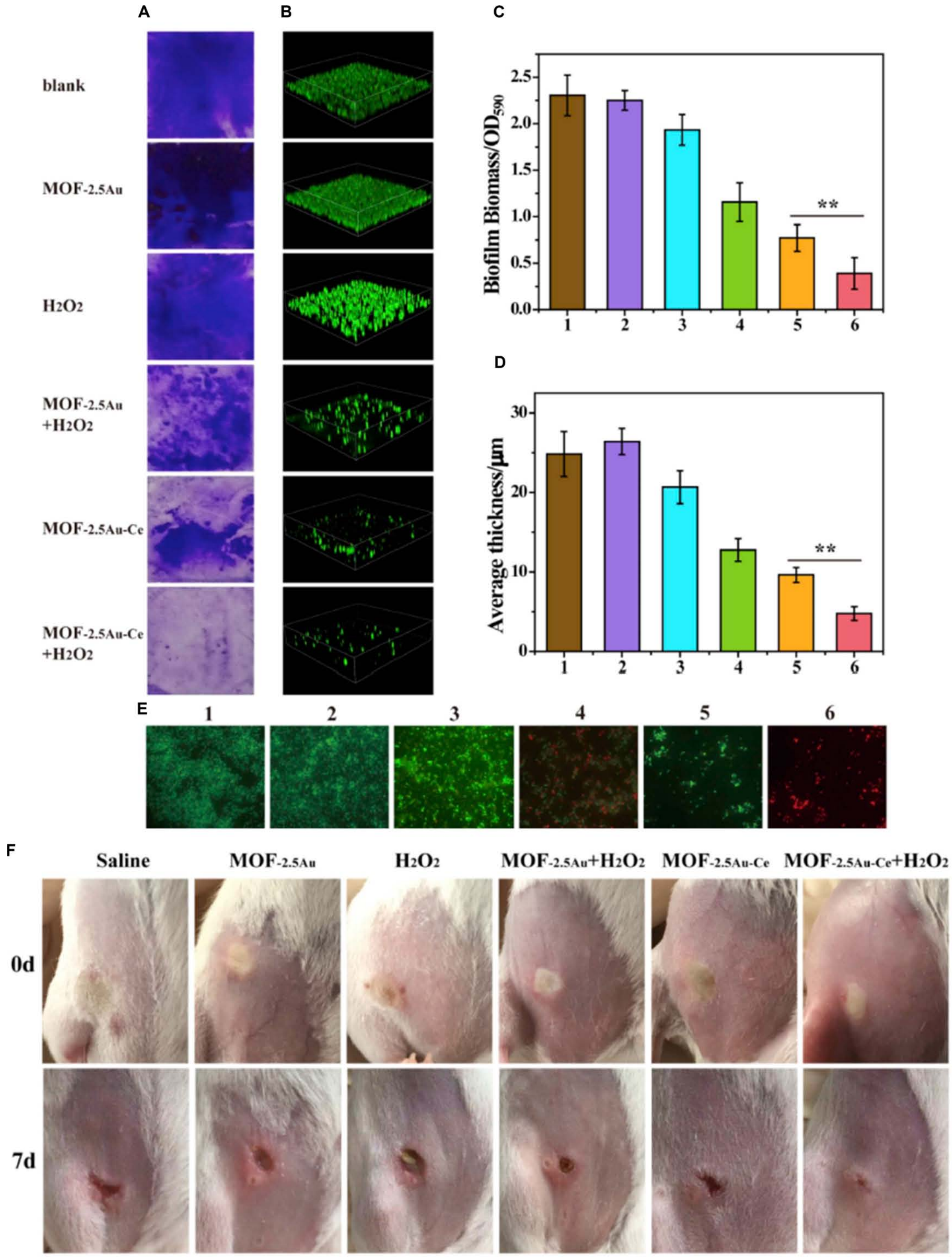

FIGURE 7 | The effect of $MOF_{-2.5Au\text{-}Ce}$ on inhibiting the formation of biofilms. **(A,C)** Crystal violet staining and **(B,D)** 3D CLSM imaging of biofilms incubated with different substances for 24 h. The biomass of biofilms was quantified by measuring OD_{590}. Image sizes of CLSM: 315 μm × 315 μm. Quantitative analysis of biofilm thickness was with the help of the Comstat 2 software. **(E)** LIVE/DEAD stain images of residual biofilms in biofilm inhibition using fluorescence microscopy. Green and red stains signified viable and dead bacteria, respectively. Scale bar = 10 μm. Group 1: control with culture medium only; group 2: treated with $MOF_{-2.5Au}$; group 3: treated with H_2O_2; group 4: treated with $MOF_{-2.5Au}$ + H_2O_2; group 5: treated with $MOF_{-2.5Au\text{-}Ce}$; group 6: treated with $MOF_{-2.5Au\text{-}Ce}$ + H_2O_2. The used nanomaterials were 200 μg/ml, and H_2O_2 was 0.5 mM. Error bars were calculated on the basis of three independent experiments. **(F)** Photographs of subcutaneous abscess in mice from the six groups at different times during the therapeutic process. Reprinted with permission from Liu et al. (2019), copyright 2019 Elsevier.

TABLE 4 | The antibacterial activities of cerium- and cerium oxide-decorated/blended materials.

Design	Morphology	Form	Dose and Conditions	Pathogens	Antimicrobial/Inhibition Activity		References
					Parameters	**Antimicrobial Efficiency**	
Ce- and CeO_2-decorated materials	composite coating	CeO_2/TiO_2 (5%, 10%, 20% CeO_2)	N/A	*S. aureus*	Sterilization rate	84%, 94%, 89%	Zhao et al., 2015
	nanorod CeO_2 coating	rod-CeO_2@Ti	N/A	*S. sanguinis*	CFU reduction	2 log	Li et al., 2019b
				F. nucleatum		1.5 log	
				P. gingivalis		2 log	
	nanocube CeO_2 coating	cube-CeO_2@Ti		*S. sanguinis*		2 log	
				F. nucleatum		> 2.5 log	
				P. gingivalis		3 log	
	nano-octahedra CeO_2 coating	octa-CeO_2@Ti		*S. sanguinis*		2 log	
				F. nucleatum		> 2.5 log	
				P. gingivalis		2 log	
	nanoparticles	MOF@CeO_2	light (638 nm, 0.65 W cm^{-2}) 5 min, 50, 200 μg/ml	*S. aureus*	Biofilm biomass reduction	> 70%, >90%	Qiu et al., 2019
	nanozymes	$MOF_{-2.5Au-Ce}$	$MOF_{-2.5Au-Ce}$ 200 μg/ml, 0.5 mM H_2O_2	*S. aureus*	Biofilm biomass reduction	66.6%	Liu et al., 2019
		$MOF_{-2.5Au-Ce}$ + H_2O_2				82.2%	
	nanozymes	DMAE	N/A	*S. aureus*	Biofilm biomass reduction (120 min)	71.4%	Chen et al., 2016
	nanocomposite	Zn–Ce/ZrP	500 mg/L	*E. coli*	Killing rate	92.60 ± 0.05%	Cai et al., 2012
				S. aureus		99.90 ± 1.35%	
	nanocomposite	CeO_2-ZnO/HNTs	100 μl	*E. coli*	Cell reduction	92%	Shu et al., 2017
	polymer	TMC-CeO_2	1 mg/100 μl	*E. coli*	MIC	100 mg/ml	Mohammad et al., 2017
					ZOI	28.2 ± 0.6 mm	
				S. aureus	MIC	100 mg/ml	
					ZOI	26.5 ± 0.6 mm	
CeO_2 blended materials	nanocomposites	Hybrid CeO_2-GO	N/A	*S. aureus*	MIC	2×10^{-5} g/ml	Kashinath et al., 2019
					MBC	5×10^{-5} g/ml	
				P. aeruginosa	MIC	1.5×10^{-5} g/ml	
					MBC	5.0×10^{-5} g/ml	
	nanofibrous mats	CeO_2-PEO/GO	5 mg/100 μl	*E. coli*	ZOI	20 mm	Bharathi and Stalin, 2019
				S. aureus		17.5 mm	
		CeO_2-PM oil-PEO/GO		*E. coli*		22.5 mm	
				S. aureus		23 mm	
CeO_2 blended materials	mixed oxide coating	ZnO and CeO_2	18.2 wt.% CeO_2	*S. aureus*	ZOI	1 mm	Evstropiev et al., 2017
			9.3 wt.% CeO_2			2 mm	
	bionanocomposite	ZnO : CeO_2 : nanocellulose : polyaniline	N/A	*B. subtilis*	MIC_{50}	10.6 g/ml	Nath et al., 2016
				E. coli		10.3 g/ml	
	composite coating	HA-CNT-CeO_2-Ag	4 wt% CNT–5 wt% CeO_2–5 wt% Ag	*E. coli*	bacterial adhesion	64.04 ± 3.97%	Pandey et al., 2018b
	coatings	CeO_2-CS	N/A	*E. faecalis*	CFU reduction	93%	Qi et al., 2019b

B. subtilis, Bacillus subtilis; CFU, colony-forming units; CNT, carbon nanotube; CS, calcium silicate; DMAE, DNase-mimetic artificial enzyme, confining AuNPs on the surface of colloidal magnetic Fe_3O_4/SiO_2 core/shell particles, which was followed by the assembly of one monolayer of Ce(IV) nitrilotriacetic acid (NTA) complexes on the exposed AuNP surfaces; E. coli, Escherichia coli; E. faecalis, Enterococcus faecalis; F. nucleatum, Fusobacterium nucleatum; HA, hydroxyapatite; HNTs, halloysite nanotubes; IC_{50}, 50% inhibiting concentration; MBC, minimum bactericidal concentration; MIC, minimum inhibitory concentration; MIC_{50}, half minimum inhibitory concentration; MOF, metal organic framework. P. aeruginosa, Pseudomonas aeruginosa; PEO/GO, polyethylene oxide/graphene oxide; P. gingivalis, Porphyromonas gingivalis; PM oil, peppermint oil; S. aureus, Staphylococcus aureus; S. sanguinis, Streptococcus sanguinis; TMC, N,N,N-trimethyl chitosan; ZrP, zirconium bis-(monohydrogen orthophosphate) monohydrate; ZOI, zone of inhibition.

were observed with the maximum ZOI against *E. coli* and *S. aureus* and showed a lower MIC value than other groups. In *in vivo* wound healing assay, CeO_2-PM oil-PEO/GO nanofibrous mats exhibited a rapid healing process in terms of promoting wound contraction, enhanced collagen deposition, and reepithelialization.

In addition, mixed oxide coating containing 90.7% ZnO NPs and 9.3% CeO_2 possessed the highest bactericidal properties against *S. aureus* under UV irradiation (Evstropiev et al., 2017). The bimodal, ZnO : CeO_2 : nanocellulose : polyaniline bionanocomposite, as potential coating agents, had a noticeable antibacterial activity with MIC_{50} values of 10.6 g/ml against *B. subtilis* and 10.3 g/ml against *E. coli* (Nath et al., 2016). Carbon nanotube (CNT) reinforcement blending with CeO_2 and Ag in HA (HA-CNT-CeO_2-Ag) had 46% bacterial adhesion reduction and 4.8 times elevated cell density in comparison with pure HA coating. Meanwhile, the physical properties such as toughness and wear resistance were also improved (Pandey et al., 2018b). The cerium oxide-incorporated calcium silicate coatings (CeO_2-CS) exhibited strong antimicrobial activity against *E. faecalis* with 93% CFU reduction (Qi et al., 2019b). The antibacterial activities of cerium- and cerium oxide-decorated/blended materials are summarized in **Table 4**.

PROBLEMS AND FUTURE PERSPECTIVES

The cytotoxicity of CeO_2 NPs can be affected by the size, shape, and surface charge of CeO_2 NPs. The smaller-sized CeO_2 NPs exhibited higher toxicity due to larger specific surface areas, higher Ce^{3+} level, and higher cellular uptake (Arumugam et al., 2015; Chen and Stephen Inbaraj, 2018). When the CeO_2 NPs achieved the same size, toxicity depended on the degree of agglomeration. Due to the various shapes of CeO_2 NPs, they showed different chemical, electrical, magnetic, and optical properties (Chen and Stephen Inbaraj, 2018). In addition, it was shown that the lower the energy barrier between CeO_2 NPs and the cell surface, the easier the adhesion to the cell surface, and the higher the cytotoxicity, the easier it is for cells to uptake CeO_2 NPs with negative zeta (Chen and Stephen Inbaraj, 2018). Yet in a phosphate condition, surface chemistry is the main reason for the antibacterial activity of CeO_2 NPs, instead of size or morphology-dependent toxicity (Sargia et al., 2017).

It was reported that CeO_2 NPs and PEGylated CeO_2 NPs could protect human dermal fibroblasts, hepatic cells, and keratinocyte HaCaT cells against cytotoxicity, genotoxicity, and oxidative stress (von Montfort et al., 2015; Singh et al., 2016; Singh and Singh, 2019). Endothelial cells could regulate the amount of intracellular CeO_2 NPs by exocytosis processes, preventing adverse effects on cells due to NP accumulation (Strobel et al., 2015). It is noteworthy that it is necessary to prevent inhalation of CeO_2 NPs. The CeO_2 NPs could penetrate the alveolar space and induce both acute and chronic inflammation in the lungs, leading to irreversible lesions (Morimoto et al., 2015; Schwotzer et al., 2017).

Whether CeO_2 NPs could promote the antibacterial properties of antibiotics is a controversial issue. Bellio et al. (2018) thought that CeO_2 NPs could act as antibiotic adjuvants to increase the effectiveness of antimicrobials. CeO_2 NPs increased bacterial outer membrane permeability, allowing the entrance of the antibiotics to increase their antibacterial activity against MDR pathogens. However, in another study, it was found that when using CeO_2 NPs and ciprofloxacin together, the antibacterial effect of ciprofloxacin could be dramatically reduced by CeO_2 NPs which may prevent ciprofloxacin from being absorbed onto the bacterial cell or interfere with ciprofloxacin activity on bacterial DNA inside the bacterial cell (Masadeh et al., 2014). When $NaCe(MoO_4)_2$ is combined with different antibiotics against different bacteria, $NaCe(MoO_4)_2$ showed a synergistical or antagonistic effect (Moura et al., 2019). Therefore, more studies associated with the combination of CeO_2 NPs and antibiotics are encouraged to be done.

It is generally believed that one of the antibacterial mechanisms is the reversible conversion between Ce(III) and Ce(IV). CeO_2 NPs with a lower Ce^{3+}/Ce^{4+} ratio show a higher catalase mimetic activity and have anticancer or antibacterial activity (Gupta et al., 2016). On the one hand, when CeO_2 NPs enter the intracellular environment, the oxidation state of CeO_2 NPs converts to a higher Ce^{3+}, indicating a net decrease of CeO_2 NPs. This is a potentially beneficial redox reaction in which harmful ROS are oxidized to a less harmful or non-harmful species. The toxicity assessment of CeO_2 NPs showed no cell death. On the other hand, significant membrane damage was observed, suggesting CeO_2 NPs may have adverse effects on the health of the cells (Szymanski et al., 2015). DNase-mimetic activity of Ce^{4+} is also one of the antibacterial mechanisms. Ce^{4+} could induce hydrolysis of a DNA oligomer into the fragments. It was reported that Ce^{4+} complexes had moderate inhibitory activity toward cancer cells by hydrolytic DNA-cleaving activities (Yang et al., 2014), but whether they could have inhibitory activity toward normal cells was still unknown. In addition, some cerium- and cerium oxide-based materials doped with Ce^{3+} showed antibacterial activity, and as the concentration of Ce^{3+} increased, the antibacterial activity increased (Bomila et al., 2018; Elayakumar et al., 2019a,b). In a phosphate condition, the surface chemistry of CeO_2 NPs with a high Ce^{3+}/Ce^{4+} ratio is altered, resulting in the loss of their intrinsic SOD activity, and this causes nutrient starvation, leading to oxidative stress in microbes. However, in this case, CeO_2 NPs with a higher Ce^{4+}/Ce^{3+} ratio did not show any antibacterial activity (Sargia et al., 2017).

To sum up, this article reviewed recent researches on cerium- and cerium oxide-based nanomaterials in the biomedical field at the present stage. This included the design of cerium- and cerium oxide-related antibacterial materials and the summary for their antibacterial effects on various species of bacteria. Cerium and cerium oxide themselves are antimicrobial agents, and the compounds containing cerium and cerium oxide received improved antimicrobial activities as well as other beneficial properties such as promoting angiogenesis, osteogenesis, and wound healing. Admittedly, researchers have made some progress in the development of various antibacterial agents and biomedical materials but far from enough. From this review, it was found that most researches were still at the level of *in vitro* experiments. In order to make cerium- and cerium oxide-related antibacterial materials obtain better application, more animal experiments and observation of long-term effects are expected. The cytotoxicity and mechanisms of new cerium- and cerium oxide-based materials need to be further investigated.

AUTHOR CONTRIBUTIONS

LW and CL designed the review article. MQ and WL wrote the manuscript. XZ, XL, YS, and YW participated and helped with the final revision of the article. All the authors read and approved the final version of the manuscript prior to submission.

FUNDING

This work was supported partly by the Health Department Research Projects in Jilin Province 2018-33-07 (LW), National Natural Science Foundation of China NSFC81400487 (LW), China Postdoctoral Science Foundation 2015M581405 and 2017T100213 (LW), and a seed grant from Jilin University School of Dentistry (LW).

REFERENCES

Abbas, F., Iqbal, J., Jan, T., Badshah, N., Mansoor, Q., and Ismail, M. (2016). Structural, morphological, Raman, optical, magnetic, and antibacterial characteristics of CeO_2 nanostructures. *Int. J. Min. Met. Mater*. 23, 102–108. doi: 10.1007/s12613-016-1216-1

Alpaslan, E., Geilich, B. M., Yazici, H., and Webster, T. J. (2017). pH-controlled cerium oxide nanoparticle inhibition of both gram-positive and gram-negative bacteria growth. *Sci. Rep*. 7, 1–12. doi: 10.1038/srep45859

Anastasiou, A. D., Nerantzaki, M., Gounari, E., Duggal, M. S., Giannoudis, P. V., Jha, A., et al. (2019). Antibacterial properties and regenerative potential of Sr^{2+} and Ce^{3+} doped fluorapatites; a potential solution for peri-implantitis. *Sci. Rep*. 9, 1–11. doi: 10.1038/s41598-019-50916-4

Artini, C., Pani, M., Carnasciali, M. M., Buscaglia, M. T., Plaisier, J. R., and Costa, G. A. (2015). Structural features of Sm-and Gd-doped ceria studied by synchrotron X-ray diffraction and μ-Raman spectroscopy. *Inorg. Chem*. 54, 4126–4137. doi: 10.1021/acs.inorgchem.5b00395

Arumugam, A., Karthikeyan, C., Haja Hameed, A. S., Gopinath, K., Gowri, S., and Karthika, V. (2015). Synthesis of cerium oxide nanoparticles using *Gloriosa superba* L. leaf extract and their structural, optical and antibacterial properties. *Mat. Sci. Eng. C Mater*. 49, 408–415. doi: 10.1016/j.msec.2015.01.042

Arunachalam, T., Karpagasundaram, M., and Rajarathinam, N. (2018). Ultrasound assisted green synthesis of cerium oxide nanoparticles using *Prosopis juliflora* leaf extract and their structural, optical and antibacterial properties. *Mater. Sci. Poland* 35, 791–798. doi: 10.1515/msp-2017-0104

Atif, M., Iqbal, S., Fakhar-E-Alam, M., Ismail, M., Mansoor, Q., Mughal, L., et al. (2019). Manganese-doped cerium oxide nanocomposite induced photodynamic therapy in MCF-7 cancer cells and antibacterial activity. *BioMed Res. Int*. 2019:7156828. doi: 10.1155/2019/7156828

Ávalos Fúnez, A., Isabel Haza, A., Mateo, D., and Morales, P. (2013). *In vitro* evaluation of silver nanoparticles on human tumoral and normal cells. *Toxicol. Mech. Method* 23, 153–160. doi: 10.3109/15376516.2012.762081

Babu, K. S., Anandkumar, M., Tsai, T. Y., Kao, T. H., Stephen Inbaraj, B., and Chen, B. H. (2014). Cytotoxicity and antibacterial activity of gold-supported cerium oxide nanoparticles. *Int. J. Nanomed*. 9, 5515–5531. doi: 10.2147/ijn.s70087

Balamurugan, A., Sudha, M., Surendhiran, S., Anandarasu, R., Ravikumar, S., and Khadar, Y. S. (2019). Hydrothermal synthesis of samarium (Sm) doped cerium oxide (CeO_2) nanoparticles: characterization and antibacterial activity. *Mater. Today: Proc*. 26, 3588–3594. doi: 10.1016/j.matpr.2019.08.217

Ballottin, D., Fulaz, S., Cabrini, F., Tsukamoto, J., Durán, N., Alves, O. L., et al. (2017). Antimicrobial textiles: biogenic silver nanoparticles against *Candida* and *Xanthomonas*. *Mater. Sci. Eng. C* 75, 582–589. doi: 10.1016/j.msec.2017.02.110

Bellio, P., Luzi, C., Mancini, A., Cracchiolo, S., Passacantando, M., Di Pietro, L., et al. (2018). Cerium oxide nanoparticles as potential antibiotic adjuvant. Effects of CeO_2 nanoparticles on bacterial outer membrane permeability. *BBA Biomembranes* 1860, 2428–2435. doi: 10.1016/j.bbamem.2018.07.002

Bharathi, B. S., and Stalin, T. (2019). Cerium oxide and peppermint oil loaded polyethylene oxide/graphene oxide electrospun nanofibrous mats as antibacterial wound dressings. *Mater. Today Commun*. 21:100664. doi: 10.1016/j.mtcomm.2019.100664

Bomila, R., Srinivasan, S., Venkatesan, A., Bharath, B., and Perinbam, K. (2018). Structural, optical and antibacterial activity studies of Ce-doped ZnO nanoparticles prepared by wet-chemical method. *Mater. Res. Innov*. 22, 379–386. doi: 10.1080/14328917.2017.1324379

Cai, X., Dai, G.-J., Tan, S.-Z., Ouyang, Y., Ouyang, Y.-S., and Shi, Q.-S. (2012). Synergistic antibacterial zinc ions and cerium ions loaded α-zirconium phosphate. *Mater. Lett*. 67, 199–201. doi: 10.1016/j.matlet.2011.09.041

Caliendo, A. M., Gilbert, D. N., Ginocchio, C. C., Hanson, K. E., May, L., Quinn, T. C., et al. (2013). Better tests, better care: improved diagnostics for infectious diseases. *Clin. Infect. Dis*. 57, S139–S170. doi: 10.1093/cid/cit578

Casadevall, A., Dadachova, E., and Pirofski, L. (2004). Passive antibody therapy for infectious diseases. *Nat. Rev. Microbiol*. 2, 695–703. doi: 10.1038/nrmicro974

Casals, E., Zeng, M., Parra-Robert, M., Fernández-Varo, G., Morales-Ruiz, M., Jiménez, W., et al. (2020). Cerium oxide nanoparticles: advances in biodistribution, toxicity, and preclinical exploration. *Small* 16:1907322. doi: 10.1002/smll.201907322

Charbgoo, F., Ahmad, M., and Darroudi, M. (2017). Cerium oxide nanoparticles: green synthesis and biological applications. *Int. J. Nanomed*. 12, 1401–1413. doi: 10.2147/ijn.s124855

Chaudhary, S., and Mehta, S. K. (2014). Selenium nanomaterials: applications in electronics, catalysis and sensors. *J. Nanosci. Nanotech*. 14, 1658–1674. doi: 10.1166/jnn.2014.9128

Chelouche, A., Touam, T., Djouadi, D., and Aksas, A. (2014). Synthesis and characterizations of new morphological ZnO and Ce-doped ZnO powders by sol–gel process. *Optik* 125, 5626–5629. doi: 10.1016/j.ijleo.2014.06.072

Chen, B. H., and Stephen Inbaraj, B. (2018). Various physicochemical and surface properties controlling the bioactivity of cerium oxide nanoparticles. *Crit. Rev. Biotechnol*. 38, 1003–1024. doi: 10.1080/07388551.2018.1426555

Chen, Y., Li, Z., and Miao, N. (2015). Polymethylmethacrylate (PMMA)/CeO_2 hybrid particles for enhanced chemical mechanical polishing performance. *Tribol. Int*. 82, 211–217. doi: 10.1016/j.triboint.2014.10.013

Chen, Z., Ji, H., Liu, C., Bing, W., Wang, Z., and Qu, X. (2016). A multinuclear metal complex based DNase-mimetic artificial enzyme: matrix cleavage for combating bacterial biofilms. *Angew. Chem. Int. Edit*. 55, 10732–10736. doi: 10.1002/anie.201605296

Chopra, I. (2007). The increasing use of silver-based products as antimicrobial agents: a useful development or a cause for concern? *J. Antimicrob. Chemoth*. 59, 587–590. doi: 10.1093/jac/dkm006

Ciobanu, G., and Harja, M. (2019). Cerium-doped hydroxyapatite/collagen coatings on titanium for bone implants. *Ceram. Int*. 45, 2852–2857. doi: 10.1016/j.ceramint.2018.07.290

Ciobanu, G., Maria Bargan, A., and Luca, C. (2015). New cerium(IV)-substituted hydroxyapatite nanoparticles: preparation and characterization. *Ceram. Int*. 41, 12192–12201. doi: 10.1016/j.ceramint.2015.06.040

Corsi, F., Caputo, F., Traversa, E., and Ghibelli, L. (2018). Not only redox: the multifaceted activity of cerium oxide nanoparticles in cancer prevention and therapy. *Front. Oncol*. 8:309. doi: 10.3389/fonc.2018.00309

Das, S., Sen, B., and Debnath, N. (2015). Recent trends in nanomaterials applications in environmental monitoring and remediation. *Environ. Sci. Pollut. R*. 22, 18333–18344. doi: 10.1007/s11356-015-5491-6

D'Costa, V. M., King, C. E., Kalan, L., Morar, M., Sung, W. W. L., Schwarz, C., et al. (2011). Antibiotic resistance is ancient. *Nature* 477, 457–461. doi: 10.1038/nature10388

Deliormanlı, A. M., Seda Vatansever, H., Yesil, H., and Özdal-Kurt, F. (2016). *In vivo* evaluation of cerium, gallium and vanadium-doped borate-based bioactive glass scaffolds using rat subcutaneous implantation model. *Ceram. Int*. 42, 11574–11583. doi: 10.1016/j.ceramint.2016.04.033

Dhall, A., and Self, W. (2018). Cerium oxide nanoparticles: a brief review of their synthesis methods and biomedical applications. *Antioxidants* 7:97. doi: 10.3390/antiox7080097

Elayakumar, K., Dinesh, A., Manikandan, A., Palanivelu, M., Kavitha, G., Prakash, S., et al. (2019a). Structural, morphological, enhanced magnetic properties and antibacterial bio-medical activity of rare earth element (REE) Cerium (Ce^{3+}) doped $CoFe_2O_4$ nanoparticles. *J. Magn. Magn. Mater*. 476, 157–165. doi: 10.1016/j.jmmm.2018.09.089

Elayakumar, K., Manikandan, A., Dinesh, A., Thanrasu, K., Raja, K. K., Kumar, R. T., et al. (2019b). Enhanced magnetic property and antibacterial biomedical activity of Ce^{3+} doped $CuFe_2O_4$ spinel nanoparticles synthesized by sol-gel method. *J. Magn. Magn. Mater*. 478, 140–147. doi: 10.1016/j.jmmm.2019.01.108

El-Shafiy, H. F., and Shebl, M. (2018). Oxovanadium (IV), cerium (III), thorium (IV) and dioxouranium (VI) complexes of 1-ethyl-4-hydroxy-3-(nitroacetyl) quinolin-2 (1H)-one: synthesis, spectral, thermal, fluorescence, DFT calculations, antimicrobial and antitumor studies. *J. Mol. Struct.* 1156, 403–417. doi: 10.1016/j.molstruc.2017.11.081

Eswar, N. K., Katkar, V. V., Ramamurthy, P. C., and Madras, G. (2015). Novel $AgBr/Ag_3PO_4$ decorated ceria nanoflake composites for enhanced photocatalytic activity toward dyes and bacteria under visible light. *Ind. Eng. Chem. Res.* 54, 8031–8042. doi: 10.1021/acs.iecr.5b01993

Evstropiev, S. K., Karavaeva, A. V., Dukelskii, K. V., Kiselev, V. M., Evstropyev, K. S., Nikonorov, N. V., et al. (2017). Transparent bactericidal coatings based on zinc and cerium oxides. *Ceram. Int*. 43, 14504–14510. doi: 10.1016/j.ceramint.2017.07.093

Fauci, A. S., and Morens, D. M. (2012). The perpetual challenge of infectious diseases. *New Engl. J. Med.* 366, 454–461. doi: 10.1056/nejmra1108296

Franci, G., Falanga, A., Galdiero, S., Palomba, L., Rai, M., Morelli, G., et al. (2015). Silver nanoparticles as potential antibacterial agents. *Molecules* 20, 8856–8874. doi: 10.3390/molecules20058856

Frieri, M., Kumar, K., and Boutin, A. (2017). Antibiotic resistance. *J. Infect. Public Heal.* 10, 369–378. doi: 10.1016/j.jiph.2016.08.007

Gagnon, J., Clift, M. J. D., Vanhecke, D., Kuhn, D. A., Weber, P., Petri-Fink, A., et al. (2015). Integrating silver compounds and nanoparticles into ceria nanocontainers for antimicrobial applications. *J. Mater. Chem. B* 3, 1760–1768. doi: 10.1039/c4tb02079k

Gagnon, J., Clift, M. J. D., Vanhecke, D., Widnersson, I. E., Abram, S.-L., Petri-Fink, A., et al. (2016). Synthesis, characterization, antibacterial activity and cytotoxicity of hollow TiO_2-coated CeO_2 nanocontainers encapsulating silver nanoparticles for controlled silver release. *J. Mater. Chem. B* 4, 1166–1174. doi: 10.1039/c5tb01917f

Gaynes, R. (2017). The discovery of penicillin—new insights after more than 75 years of clinical use. *Emerg. Infect. Dis.* 23, 849–853. doi: 10.3201/eid2305.161556

Goh, Y., Akram, M., Alshemary, A., and Hussain, R. (2016). Antibacterial polylactic acid/chitosan nanofibers decorated with bioactive glass. *Appl. Surf. Sci.* 387, 1–7. doi: 10.1016/j.apsusc.2016.06.054

Goh, Y. F., Alshemary, A. Z., Akram, M., Kadir, M. R. A., and Hussain, R. (2014). *In-vitro* characterization of antibacterial bioactive glass containing ceria. *Ceram. Int.* 40, 729–737. doi: 10.1016/j.ceramint.2013.06.062

Gopi, D., Ramya, S., Rajeswari, D., Karthikeyan, P., and Kavitha, L. (2014). Strontium, cerium co-substituted hydroxyapatite nanoparticles: synthesis, characterization, antibacterial activity towards prokaryotic strains and in vitro studies. *Colloid. Surface A* 451, 172–180. doi: 10.1016/j.colsurfa.2014.03.035

Gopinath, K., Karthika, V., Sundaravadivelan, C., Gowri, S., and Arumugam, A. (2015). Mycogenesis of cerium oxide nanoparticles using *Aspergillus niger* culture filtrate and their applications for antibacterial and larvicidal activities. *J. Nanostruct. Chem.* 5, 295–303. doi: 10.1007/s40097-015-0161-2

Gupta, A., Das, S., Neal, C. J., and Seal, S. (2016). Controlling the surface chemistry of cerium oxide nanoparticles for biological applications. *J. Mater. Chem. B* 4, 3195–3202. doi: 10.1039/c6tb00396f

Hou, J., You, G., Xu, Y., Wang, C., Wang, P., Miao, L., et al. (2015). Effects of CeO_2 nanoparticles on biological nitrogen removal in a sequencing batch biofilm reactor and mechanism of toxicity. *Bioresour. Technol.* 191, 73–78. doi: 10.1016/j.biortech.2015.04.123

Hu, T., Xiao, S., Yang, H., Chen, L., and Chen, Y. (2018). Cerium oxide as an efficient electron extraction layer for p–i–n structured perovskite solar cells. *Chem. Commun.* 54, 471–474. doi: 10.1039/c7cc08657a

Huang, F., Wang, J., Chen, W., Wan, Y., Wang, X., Cai, N., et al. (2018). Synergistic peroxidase-like activity of CeO_2-coated hollow Fe_3O_4 nanocomposites as an enzymatic mimic for low detection limit of glucose. *J. Taiwan Inst. Chem. E.* 83, 40–49. doi: 10.1016/j.jtice.2017.12.011

Huang, X., Li, L.-D., Lyu, G.-M., Shen, B.-Y., Han, Y.-F., Shi, J.-L., et al. (2018). Chitosan-coated cerium oxide nanocubes accelerate cutaneous wound healing by curtailing persistent inflammation. *Inorg. Chem. Front.* 5, 386–393. doi: 10.1039/c7qi00707h

Hui, A., Liu, J., and Ma, J. (2016). Synthesis and morphology-dependent antimicrobial activity of cerium doped flower-shaped ZnO crystallites under visible light irradiation. *Colloid. Surface. A* 506, 519–525. doi: 10.1016/j.colsurfa.2016.07.016

Ivask, A., Juganson, K., Bondarenko, O., Mortimer, M., Aruoja, V., Kasemets, K., et al. (2014). Mechanisms of toxic action of Ag, ZnO and CuO nanoparticles to selected ecotoxicological test organisms and mammalian cells *in vitro*: a comparative review. *Nanotoxicology* 8, 57–71. doi: 10.3109/17435390.2013.855831

Jayaseelan, C., Rahuman, A. A., Roopan, S. M., Kirthi, A. V., Venkatesan, J., Kim, S.-K., et al. (2013). Biological approach to synthesize TiO_2 nanoparticles using *Aeromonas hydrophila* and its antibacterial activity. *Spectrochim. Acta A* 107, 82–89. doi: 10.1016/j.saa.2012.12.083

Jones, J. R. (2015). Reprint of: review of bioactive glass: from hench to hybrids. *Acta Biomater.* 23, S53–S82. doi: 10.1016/j.actbio.2015.07.019

Jones, K. E., Patel, N. G., Levy, M. A., Storeygard, A., Balk, D., Gittleman, J. L., et al. (2008). Global trends in emerging infectious diseases. *Nature* 451, 990–993. doi: 10.1038/nature06536

Kargozar, S., Baino, F., Hoseini, S. J., Hamzehlou, S., Darroudi, M., Verdi, J., et al. (2018). Biomedical applications of nanoceria: new roles for an old player. *Nanomedicine* 13, 3051–3069. doi: 10.2217/nnm-2018-0189

Kashinath, L., Namratha, K., and Byrappa, K. (2019). Microwave mediated synthesis and characterization of CeO_2-GO hybrid composite for removal of chromium ions and its antibacterial efficiency. *J. Environ. Sci.* 76, 65–79. doi: 10.1016/j.jes.2018.03.027

Kasinathan, K., Kennedy, J., Elayaperumal, M., Henini, M., and Malik, M. (2016). Photodegradation of organic pollutants RhB dye using UV simulated sunlight on ceria based TiO_2 nanomaterials for antibacterial applications. *Sci. rep.* 6, 1–12. doi: 10.1038/srep38064

Kaygusuz, H., Torlak, E., Akın-Evingür, G., Özen, Ý, von Klitzing, R., and Erim, F. B. (2017). Antimicrobial cerium ion-chitosan crosslinked alginate biopolymer films: a novel and potential wound dressing. *Int. J. Biol. Macromol.* 105, 1161–1165. doi: 10.1016/j.ijbiomac.2017.07.144

Khadar, Y. S., Balamurugan, A., Devarajan, V. P., Subramanian, R., and Dinesh Kumar, S. (2019). Synthesis, characterization and antibacterial activity of cobalt doped cerium oxide (CeO_2: Co) nanoparticles by using hydrothermal method. *J. Mater. Res. Technol.* 8, 267–274. doi: 10.1016/j.jmrt.2017.12.005

Khan, S. T., Al-Khedhairy, A. A., and Musarrat, J. (2015). ZnO and TiO_2 nanoparticles as novel antimicrobial agents for oral hygiene: a review. *J. Nanopart. Res.* 17:276. doi: 10.1007/s11051-015-3074-6

Khot, L. R., Sankaran, S., Maja, J. M., Ehsani, R., and Schuster, E. W. (2012). Applications of nanomaterials in agricultural production and crop protection: a review. *Crop Prot.* 35, 64–70. doi: 10.1016/j.cropro.2012.01.007

Krishnamoorthy, K., Veerapandian, M., Zhang, L.-H., Yun, K., and Kim, S. J. (2014). Surface chemistry of cerium oxide nanocubes: toxicity against pathogenic bacteria and their mechanistic study. *J. Ind. Eng. Chem.* 20, 3513–3517. doi: 10.1016/j.jiec.2013.12.043

Kumar, K. M., Mahendhiran, M., Diaz, M. C., Hernandez-Como, N., Hernandez-Eligio, A., Torres-Torres, G., et al. (2018). Green synthesis of Ce^{3+} rich CeO_2 nanoparticles and its antimicrobial studies. *Mater. Lett.* 214, 15–19. doi: 10.1016/j.matlet.2017.11.097

Lee, K. M., Lai, C. W., Ngai, K. S., and Juan, J. C. (2016). Recent developments of zinc oxide based photocatalyst in water treatment technology: a review. *Water Res.* 88, 428–448. doi: 10.1016/j.watres.2015.09.045

Li, L., Zhu, B., Zhang, J., Yan, C., and Wu, Y. (2018). Electrical properties of nanocube CeO_2 in advanced solid oxide fuel cells. *Int. J. Hydrogen. Energ.* 43, 12909–12916. doi: 10.1016/j.ijhydene.2018.05.120

Li, W., Qi, M., Sun, X., Chi, M., Wan, Y., Zheng, X., et al. (2020). Novel dental adhesive containing silver exchanged EMT zeolites against cariogenic biofilms to combat dental caries. *Micropor. Mesopor. Mat.* 299:110113. doi: 10.1016/j.micromeso.2020.110113

Li, X., Qi, M., Li, C., Dong, B., Wang, J., Weir, M. D., et al. (2019a). Novel nanoparticles of cerium-doped zeolitic imidazolate frameworks with dual benefits of antibacterial and anti-inflammatory functions against periodontitis. *J. Mater. Chem. B* 7, 6955–6971. doi: 10.1039/c9tb01743g

Li, X., Qi, M., Sun, X., Weir, M. D., Tay, F. R., Oates, T. W., et al. (2019b). Surface treatments on titanium implants via nanostructured ceria for antibacterial and anti-inflammatory capabilities. *Acta Biomater.* 94, 627–643. doi: 10.1016/j.actbio.2019.06.023

Li, Y., Zhang, W., Niu, J., and Chen, Y. (2012). Mechanism of photogenerated reactive oxygen species and correlation with the antibacterial properties of engineered metal-oxide nanoparticles. *ACS Nano* 6, 5164–5173. doi: 10.1021/nn300934k

Liu, Z., Wang, F., Ren, J., and Qu, X. (2019). A series of MOF/Ce-based nanozymes with dual enzyme-like activity disrupting biofilms and hindering recolonization of bacteria. *Biomaterials* 208, 21–31. doi: 10.1016/j.biomaterials.2019.04.007

Malleshappa, J., Nagabhushana, H., Sharma, S. C., Vidya, Y. S., Anantharaju, K. S., Prashantha, S. C., et al. (2015). Leucas aspera mediated multifunctional CeO_2 nanoparticles: structural, photoluminescent, photocatalytic and antibacterial properties. *Spectrochim. Acta Part A* 149, 452–462. doi: 10.1016/j.saa.2015.04.073

Masadeh, M. M., Karasneh, G. A., Al-Akhras, M. A., Albiss, B. A., Aljarah, K. M., Al-azzam Sayer, I., et al. (2014). Cerium oxide and iron oxide nanoparticles abolish the antibacterial activity of ciprofloxacin against gram positive and gram negative biofilm bacteria. *Cytotechnology* 67, 427–435. doi: 10.1007/s10616-014-9701-8

Matsuzaki, S., Rashel, M., Uchiyama, J., Sakurai, S., Ujihara, T., Kuroda, M., et al. (2005). Bacteriophage therapy: a revitalized therapy against bacterial infectious diseases. *J. Infect. Chemother.* 11, 211–219. doi: 10.1007/s10156-005-0408-9

Mekala, R., Rajendran, V., and Deepa, B. (2018). Effect of cerium doped Baddeleyite on their antibacterial activity by co-precipitation method. IOP conference series. *Mater. Sci. Eng.* 360:012014. doi: 10.1088/1757-899x/360/1/012014

Mishra, P. K., Mishra, H., Ekielski, A., Talegaonkar, S., and Vaidya, B. (2017). Zinc oxide nanoparticles: a promising nanomaterial for biomedical applications. *Drug Discov. Today* 22, 1825–1834. doi: 10.1016/j.drudis.2017.08.006

Mishra, S., Priyadarshinee, M., Debnath, A. K., Muthe, K. P., Mallick, B. C., Das, N., et al. (2020). Rapid microwave assisted hydrothermal synthesis cerium vanadate nanoparticle and its photocatalytic and antibacterial studies. *J. Phys. Chem. Solids* 137:109211. doi: 10.1016/j.jpcs.2019.109211

Mitragotri, S., Anderson, D. G., Chen, X., Chow, E. K., Ho, D., Kabanov, A. V., et al. (2015). Accelerating the translation of nanomaterials in biomedicine. *ACS Nano* 9, 6644–6654. doi: 10.1021/acsnano.5b03569

Mohammad, F., Arfin, T., and Al-Lohedan, H. A. (2017). Enhanced biological activity and biosorption performance of trimethyl chitosan-loaded cerium oxide particles. *J. Ind. Eng.Chem.* 45, 33–43. doi: 10.1016/j.jiec.2016.08.029

Moongraksathum, B., and Chen, Y. W. (2018). Anatase TiO_2 co-doped with silver and ceria for antibacterial application. *Catal. Today* 310, 68–74. doi: 10.1016/j.cattod.2017.05.087

Morais, D. S., Fernandes, S., Gomes, P. S., Fernandes, M. H., Sampaio, P., Ferraz, M. P., et al. (2015). Novel cerium doped glass-reinforced hydroxyapatite with antibacterial and osteoconductive properties for bone tissue regeneration. *Biomed. Mater.* 10:055008. doi: 10.1088/1748-6041/10/5/055008

Morimoto, Y., Izumi, H., Yoshiura, Y., Tomonaga, T., Oyabu, T., Myojo, T., et al. (2015). Pulmonary toxicity of well-dispersed cerium oxide nanoparticles following intratracheal instillation and inhalation. *J. Nanopart. Res.* 17:442. doi: 10.1007/s11051-015-3249-1

Moura, J. V. B., Freitas, T. S., Cruz, R. P., Pereira, R. L. S., Silva, A. R. P., Santos, A. T. L., et al. (2019). Antibacterial properties and modulation analysis of antibiotic activity of NaCe $(MoO_4)_2$ microcrystals. *Microb. Pathogen.* 126, 258–262. doi: 10.1016/j.micpath.2018.11.019

Muthukumaran, P., Raju, C. V., Sumathi, C., Ravi, G., Solairaj, D., Rameshthangam, P., et al. (2016). Cerium doped nickel-oxide nanostructures for riboflavin biosensing and antibacterial applications. *New J. Chem.* 40, 2741–2748. doi: 10.1039/c5nj03539b

Nath, B. K., Chaliha, C., Kalita, E., and Kalita, M. C. (2016). Synthesis and characterization of ZnO:CeO_2:nanocellulose:PANI bionanocomposite. A bimodal agent for arsenic adsorption and antibacterial action. *Carbohyd. Polym.* 148, 397–405. doi: 10.1016/j.carbpol.2016.03.091

Naz, S., Beach, J., Heckert, B., Tummala, T., Pashchenko, O., Banerjee, T., et al. (2017). Cerium oxide nanoparticles: a "radical" approach to neurodegenerative disease treatment. *Nanomedicine* 12, 545–553. doi: 10.2217/nnm-2016-0399

Negi, K., Umar, A., Chauhan, M. S., and Akhtar, M. S. (2019). Ag/CeO_2 nanostructured materials for enhanced photocatalytic and antibacterial applications. *Ceram. Int.* 45, 20509–20517. doi: 10.1016/j.ceramint.2019.07.030

Nigam, A., Gupta, D., and Sharma, A. (2014). Treatment of infectious disease: beyond antibiotics. *Microbiol. Res.* 169, 643–651. doi: 10.1016/j.micres.2014.02.009

Nyoka, M., Choonara, Y. E., Kumar, P., Kondiah, P. P., and Pillay, V. (2020). Synthesis of cerium oxide nanoparticles using various methods: implications for biomedical applications. *Nanomaterials* 10:242. doi: 10.3390/nano10020242

Palmer, L. D., and Skaar, E. P. (2016). Transition metals and virulence in bacteria. *Annu. Rev. Genet.* 50, 67–91. doi: 10.1146/annurev-genet-120215-035146

Pandey, A., Midha, S., Sharma, R. K., Maurya, R., Nigam, V. K., Ghosh, S., et al. (2018a). Antioxidant and antibacterial hydroxyapatite-based biocomposite for orthopedic applications. *Mater. Sci. Eng. C* 88, 13–24. doi: 10.1016/j.msec.2018.02.014

Pandey, A., Patel, A., Ariharan, S., Kumar, V., Sharma, R., Kanhed, S., et al. (2018b). Enhanced tribological and bacterial resistance of carbon nanotube with ceria- and silver-incorporated hydroxyapatite biocoating. *Nanomaterials* 8:363. doi: 10.3390/nano8060363

Panneerselvam, R., Anandhan, N., Gopu, G., Amali Roselin, A., Ganesan, K. P., and Marimuthu, T. (2020). Impact of different transition metal ions in the structural, mechanical, optical, chemico-physical and biological properties of nanoHydroxyapatite. *Appl. Surf. Sci.* 506:144802. doi: 10.1016/j.apsusc.2019.144802

Patil, S. N., Paradeshi, J. S., Chaudhari, P. B., Mishra, S. J., and Chaudhari, B. L. (2016). Bio-therapeutic potential and cytotoxicity assessment of pectin-mediated synthesized nanostructured cerium oxide. *Appl. Biochem. Biotech.* 180, 638–654. doi: 10.1007/s12010-016-2121-9

Pelletier, D. A., Suresh, A. K., Holton, G. A., McKeown, C. K., Wang, W., Gu, B., et al. (2010). Effects of engineered cerium oxide nanoparticles on bacterial growth and viability. *Appl. Environ. Microb.* 76, 7981–7989. doi: 10.1128/aem.00650-10

Phatai, P., Futalan, C. M., Utara, S., Khemthong, P., and Kamonwannasit, S. (2018). Structural characterization of cerium-doped hydroxyapatite nanoparticles synthesized by an ultrasonic-assisted sol-gel technique. *Results Phys.* 10, 956–963. doi: 10.1016/j.rinp.2018.08.012

Priyadarshini, B., and Vijayalakshmi, U. (2018). Development of cerium and silicon co-doped hydroxyapatite nanopowder and its in vitro biological studies for bone regeneration applications. *Adv. Powder Technol.* 29, 2792–2803. doi: 10.1016/j.apt.2018.07.028

Qi, L., Xu, Z., Jiang, X., Hu, C., and Zou, X. (2004). Preparation and antibacterial activity of chitosan nanoparticles. *Carbohyd. Res.* 339, 2693–2700. doi: 10.1016/j.carres.2004.09.007

Qi, M., Li, X., Sun, X., Li, C., Tay, F. R., Weir, M. D., et al. (2019). Novel nanotechnology and near-infrared photodynamic therapy to kill periodontitis-related biofilm pathogens and protect the periodontium. *Dent. Mater.* 35, 1665–1681. doi: 10.1016/j.dental.2019.08.115

Qi, S., Wu, J., Xu, Y., Zhang, Y., Wang, R., Li, K., et al. (2019). Chemical stability and antimicrobial activity of plasma-sprayed cerium oxide–incorporated calcium silicate coating in dental implants. *Implant Dent.* 28, 564–570. doi: 10.1097/id.0000000000000937

Qiu, H., Pu, F., Liu, Z., Deng, Q., Sun, P., Ren, J., et al. (2019). Depriving bacterial adhesion-related molecule to inhibit biofilm formation using CeO_2-decorated metal-organic frameworks. *Small* 15:1902522. doi: 10.1002/smll.201902522

Rahdar, A., Aliahmad, M., Samani, M., HeidariMajd, M., and Abu Bin Hasan Susan, M. (2019). Synthesis and characterization of highly efficacious Fe-doped ceria nanoparticles for cytotoxic and antifungal activity. *Ceram. Int*. 45, 7950–7955. doi: 10.1016/j.ceramint.2019.01.108

Ramalingam, B., Parandhaman, T., and Das, S. K. (2016). Antibacterial effects of biosynthesized silver nanoparticles on surface ultrastructure and nanomechanical properties of Gram-negative bacteria viz. *Escherichia coli* and *Pseudomonas aeruginosa*. *ACS Appl. Mater. Inter*. 8, 4963–4976. doi: 10.1021/acsami.6b00161

Ravishankar, T. N., Ramakrishnappa, T., Nagaraju, G., and Rajanaika, H. (2015). Synthesis and characterization of CeO_2 nanoparticles via solution combustion method for photocatalytic and antibacterial activity studies. *ChemistryOpen* 4, 146–154. doi: 10.1002/open.201402046

Rodhe, Y., Skoglund, S., Odnevall Wallinder, I., Potácová, Z., and Möller, L. (2015). Copper-based nanoparticles induce high toxicity in leukemic HL60 cells. *Toxicol. Vitro* 29, 1711–1719. doi: 10.1016/j.tiv.2015.05.020

Roudbaneh, S. Z. K., Kahbasi, S., Sohrabi, M. J., Hasan, A., Salihi, A., Mirzaie, A., et al. (2019). Albumin binding, antioxidant and antibacterial effects of cerium oxide nanoparticles. *J. Mol. Liq*. 296:111839. doi: 10.1016/j.molliq.2019.111839

Sang, Y. L., Lin, X. S., Li, X. C., Liu, Y. H., and Zhang, X. H. (2015). Synthesis, crystal structure and antibacterial activity of a novel phenolato-and peroxo-bridged dinuclear cerium (IV) complex with tripodal Schiff bases. *Inorg. Chem. Commun*. 62, 115–118. doi: 10.1016/j.inoche.2015.11.003

Sang, Y. L., Lin, X. S., Li, X. C., Liu, Y. H., and Zhang, X. H. (2017). Synthesis, crystal structure, and antibacterial activity of a mononuclear cerium (III) complex derived from tris (2-((5-chlorosalicylidene) amino) ethyl) amine. *Inorg. Nano Met. Chem*. 47, 86–90. doi: 10.1080/15533174.2016.1149725

Sanhueza, F., Valdebenito, E., Udayabhaskar, R., Salvo, C., Sahlevani, S. F., Elgueta, E., et al. (2019). Effect of ultrasonic sonication time on the structural, optical and antibacterial properties of ceria nanostructures. *Mater. Res. Express* 6:095055. doi: 10.1088/2053-1591/ab2e6c

Sargia, B., Shah, J., Singh, R., Arya, H., Shah, M., Karakoti, A. S., et al. (2017). Phosphate-dependent modulation of antibacterial strategy: a redox state-controlled toxicity of cerium oxide nanoparticles. *Bull. Mater. Sci.* 40, 1231–1240. doi: 10.1007/s12034-017-1480-3

Schwotzer, D., Ernst, H., Schaudien, D., Kock, H., Pohlmann, G., Dasenbrock, C., et al. (2017). Effects from a 90-day inhalation toxicity study with cerium oxide and barium sulfate nanoparticles in rats. *Part. Fibre Toxicol.* 14:23. doi: 10.1186/s12989-017-0204-6

Scida, K., Stege, P. W., Haby, G., Messina, G. A., and García, C. D. (2011). Recent applications of carbon-based nanomaterials in analytical chemistry: critical review. *Anal. Chim. Acta* 691, 6–17. doi: 10.1016/j.aca.2011.02.025

Seal, S., Jeyaranjan, A., Neal, C. J., Kumar, U., Sakthivel, T. S., and Sayle, D. C. (2020). Engineered defects in cerium oxides: tuning chemical reactivity for biomedical, environmental, & energy applications. *Nanoscale* 12, 6879–6899. doi: 10.1039/D0NR01203C

Selvaraj, V., Manne, N. D., Arvapalli, R., Rice, K. M., Nandyala, G., Fankenhanel, E., et al. (2015). Effect of cerium oxide nanoparticles on sepsis induced mortality and NF-κB signaling in cultured macrophages. *Nanomedicine* 10, 1275–1288. doi: 10.2217/nnm.14.205

Senthilkumar, R. P., Bhuvaneshwari, V., Malayaman, V., Chitra, G., Ranjithkumar, R., Dinesh, K. P. B., et al. (2019). Biogenic method of cerium oxide nanoparticles synthesis using wireweed (Sida acuta Burm.f.) and its antibacterial activity against *Escherichia coli*. *Mater. Res. Express* 6:105026. doi: 10.1088/2053-1591/ab37b9

Senthilkumar, R. P., Bhuvaneshwari, V., Ranjithkumar, R., Sathiyavimal, S., Malayaman, V., and Chandarshekar, B. (2017). Synthesis, characterization and antibacterial activity of hybrid chitosan-cerium oxide nanoparticles: as a bionanomaterials. *Int. J. Biol. Macromol.* 104, 1746–1752. doi: 10.1016/j.ijbiomac.2017.03.139

Shu, Z., Zhang, Y., Ouyang, J., and Yang, H. (2017). Characterization and synergetic antibacterial properties of ZnO and CeO_2 supported by halloysite. *Appl. Surf. Sci.* 420, 833–838. doi: 10.1016/j.apsusc.2017.05.219

Shuhailath, K. A., Linsha, V., Kumar, S. N., Babitha, K. B., Peer Mohamed, A. A., and Ananthakumar, S. (2016). Photoactive, antimicrobial CeO_2 decorated AlOOH/PEI hybrid nanocomposite: a multifunctional catalytic-sorbent for lignin and organic dye. *RSC Adv*. 6, 54357–54370. doi: 10.1039/c6ra07836b

Singh, R., Karakoti, A. S., Self, W., Seal, S., and Singh, S. (2016). Redox-sensitive cerium oxide nanoparticles protect human keratinocytes from oxidative stress induced by glutathione depletion. *Langmuir* 32, 12202–12211. doi: 10.1021/acs.langmuir.6b03022

Singh, R., and Singh, S. (2019). Redox-dependent catalase mimetic cerium oxide-based nanozyme protect human hepatic cells from 3-AT induced acatalasemia. *Colloid. Surface B* 175, 625–635. doi: 10.1016/j.colsurfb.2018.12.042

Sirelkhatim, A., Mahmud, S., Seeni, A., Kaus, N. H. M., Ann, L. C., Bakhori, S. K. M., et al. (2015). Review on zinc oxide nanoparticles: antibacterial activity and toxicity mechanism. *Nano Micro Lett.* 7, 219–242. doi: 10.1007/s40820-015-0040-x

Stoor, P., Söderling, E., and Salonen, J. I. (1998). Antibacterial effects of a bioactive glass paste on oral microorganisms. *Acta Odontol. Scand.* 56, 161–165. doi: 10.1080/000163598422901

Strobel, C., Oehring, H., Herrmann, R., Förster, M., Reller, A., and Hilger, I. (2015). Fate of cerium dioxide nanoparticles in endothelial cells: exocytosis. *J. Nanopart. Res.* 17:206. doi: 10.1007/s11051-015-3007-4

Sumaoka, J., Azuma, Y., and Komiyama, M. (1998). Enzymatic manipulation of the fragments obtained by cerium(IV)-induced DNA scission: characterization of hydrolytic termini. *Chem. Eur. J.* 4, 205–209. doi: 10.1002/(sici)1521-3765(19980210)4:2<205::aid-chem205>3.0.co;2-d

Sun, Q., Fu, Z., and Yang, Z. (2018). Effects of rare-earth doping on the ionic conduction of CeO_2 in solid oxide fuel cells. *Ceram. Int.* 44, 3707–3711. doi: 10.1016/j.ceramint.2017.11.149

Surendra, T. V., and Roopan, S. M. (2016). Photocatalytic and antibacterial properties of phytosynthesized CeO_2 NPs using *Moringa oleifera* peel extract. *J. Photoch. Photobio. B* 161, 122–128. doi: 10.1016/j.jphotobiol.2016.05.019

Suresh, S. (2013). Semiconductor nanomaterials, methods and applications: a review. *Nanosci. Nanotechno.* 3, 62–74. doi: 10.5923/j.nn.20130303.06

Szymanski, C. J., Munusamy, P., Mihai, C., Xie, Y., Hu, D., Gilles, M. K., et al. (2015). Shifts in oxidation states of cerium oxide nanoparticles detected inside intact hydrated cells and organelles. *Biomaterials* 62, 147–154. doi: 10.1016/j.biomaterials.2015.05.042

Thill, A., Zeyons, O., Spalla, O., Chauvat, F., Rose, J., Auffan, M., et al. (2006). Cytotoxicity of CeO_2 nanoparticles for *Escherichia coli*. Physico-chemical insight of the cytotoxicity mechanism. *Environ. Sci. Technol.* 40, 6151–6156. doi: 10.1021/es060999b

Truffault, L., Rodrigues, D. F., Salgado, H. R. N., Santilli, C. V., and Pulcinelli, S. H. (2016). Loaded Ce-Ag organic-inorganic hybrids and their antibacterial activity. *Colloid. Surface B* 147, 151–160. doi: 10.1016/j.colsurfb.2016.07.061

Vanitha, M., Joni, I. M., Camellia, P., and Balasubramanian, N. (2018). Tailoring the properties of cerium doped zinc oxide/reduced graphene oxide composite: characterization, photoluminescence study, antibacterial activity. *Ceram. Int.* 44, 19725–19734. doi: 10.1016/j.ceramint.2018.07.226

von Montfort, C., Alili, L., Teuber-Hanselmann, S., and Brenneisen, P. (2015). Redox-active cerium oxide nanoparticles protect human dermal fibroblasts from PQ-induced damage. *Redox Biol.* 4, 1–5. doi: 10.1016/j.redox.2014.11.007

Walkey, C., Das, S., Seal, S., Erlichman, J., Heckman, K., Ghibelli, L., et al. (2015). Catalytic properties and biomedical applications of cerium oxide nanoparticles. *Environ. Sci. Nano* 2, 33–53. doi: 10.1039/c4en00138a

Wang, L., He, H., Yu, Y., Sun, L., Liu, S., Zhang, C., et al. (2014). Morphology-dependent bactericidal activities of Ag/CeO_2 catalysts against *Escherichia coli*. *J. Inorg. Biochem.* 135, 45–53. doi: 10.1016/j.jinorgbio.2014.02.016

Wang, M., Hu, M., Hu, B., Guo, C., Song, Y., Jia, Q., et al. (2019). Bimetallic cerium and ferric oxides nanoparticles embedded within mesoporous carbon matrix: electrochemical immunosensor for sensitive detection of carbohydrate antigen 19-9. *Biosens. Bioelectron.* 135, 22–29. doi: 10.1016/j.bios.2019.04.018

Wang, Y. Z., Wu, Y. S., Xue, X. X., Yang, H., and Liu, Z. H. (2017). Microstructure and antibacterial activity of ions (Ce, Y, or B)-doped Zn-TiO_2: a comparative study. *Mater. Technol.* 32, 310–320. doi: 10.1080/10667857.2016.1215089

Wang, Y. Z., Wu, Y. S., Yang, H., Wang, M., Shi, X. G., Wang, C., et al. (2018). Effect of calcination temperature on the microstructure and antimicrobial activity of boron and cerium co-doped titania nanomaterials. *Mater. Technol.* 33, 48–56. doi: 10.1080/10667857.2017.1389051

Wu, H., Moser, C., Wang, H.-Z., Høiby, N., and Song, Z.-J. (2015). Strategies for combating bacterial biofilm infections. *Int. J. Oral Sci.* 7, 1–7. doi: 10.1038/ijos.2014.65

Wyszogrodzka, G., Marszałek, B., Gil, B., and Dorożyński, P. (2016). Metal-organic frameworks: mechanisms of antibacterial action and potential applications. *Drug Discov. Today* 21, 1009–1018. doi: 10.1016/j.drudis.2016.04.009

Xu, C., and Qu, X. (2014). Cerium oxide nanoparticle: a remarkably versatile rare earth nanomaterial for biological applications. *NPG Asia Mater.* 6:e90. doi: 10.1038/am.2013.88

Yadav, L. R., Manjunath, K., Archana, B., Madhu, C., Naika, H. R., Nagabhushana, H., et al. (2016). Fruit juice extract mediated synthesis of CeO_2 nanoparticles for antibacterial and photocatalytic activities. *EPJ Plus* 131:154. doi: 10.1140/epjp/i2016-16154-y

Yang, J. W., Lin, Y. L., Dong, C., Zhou, C. Q., Chen, J. X., Wang, B., et al. (2014). Synthesis, hydrolytic DNA-cleaving activities and cytotoxicities of EDTA analogue-tethered pyrrole-polyamide dimer-based Ce(IV) complexes. *Eur. J. Med. Chem.* 87, 168–174. doi: 10.1016/j.ejmech.2014.09.057

Yuan, Q., Qin, C., Wu, J., Xu, A., Zhang, Z., Liao, J., et al. (2016). Synthesis and characterization of cerium-doped hydroxyapatite/polylactic acid composite coatings on metal substrates. *Mater. Chem. Phys.* 182, 365–371. doi: 10.1016/j.matchemphys.2016.07.044

Zeyons, O., Thill, A., Chauvat, F., Menguy, N., Cassier-Chauvat, C., Oréar, C., et al. (2009). Direct and indirect CeO_2 nanoparticles toxicity for *Escherichia coli* and *Synechocystis*. *Nanotoxicology* 3, 284–295. doi: 10.3109/17435390903305260

Zhang, M., Zhang, C., Zhai, X., Luo, F., Du, Y., and Yan, C. (2019). Antibacterial mechanism and activity of cerium oxide nanoparticles. *Sci. China Mater.* 62, 1727–1739. doi: 10.1007/s40843-019-9471-7

Zhang, X., Hou, F., Yang, Y., Wang, Y., Liu, N., Chen, D., et al. (2017). A facile synthesis for cauliflower like CeO_2 catalysts from Ce-BTC precursor and their catalytic performance for CO oxidation. *Appl. Surf. Sci.* 423, 771–779. doi: 10.1016/j.apsusc.2017.06.235

Zhang, Y., Wang, F., Liu, C., Wang, Z., Kang, L., Huang, Y., et al. (2018). Nanozyme decorated metal–organic frameworks for enhanced photodynamic therapy. *ACS Nano* 12, 651–661. doi: 10.1021/acsnano.7b07746

Zhao, X., Liu, G., Zheng, H., Cao, H., and Liu, X. (2015). Dose-dependent effects of CeO_2 on microstructure and antibacterial property of plasma-sprayed TiO_2 coatings for orthopedic application. *J. Therm. Spray Techn.* 24, 401–409. doi: 10.1007/s11666-014-0179-x

Conflict of Interest: The authors declare that the research was conducted in the absence of any commercial or financial relationships that could be construed as a potential conflict of interest.